Supporting Information

Designable Assembly of Atomically Precise Al_4O_4 Cubane Supported Mesoporous Heterometallic Architectures

Ya-Jie Liu, Ying-Hua Yu, Yi-Fan Sun, Wei-Hui Fang* and Jian Zhang*

Table of Content

1. The supertetrahedral clusters and 2-fold interpenetrated frameworks in AlOC-99 to AlOC-108.

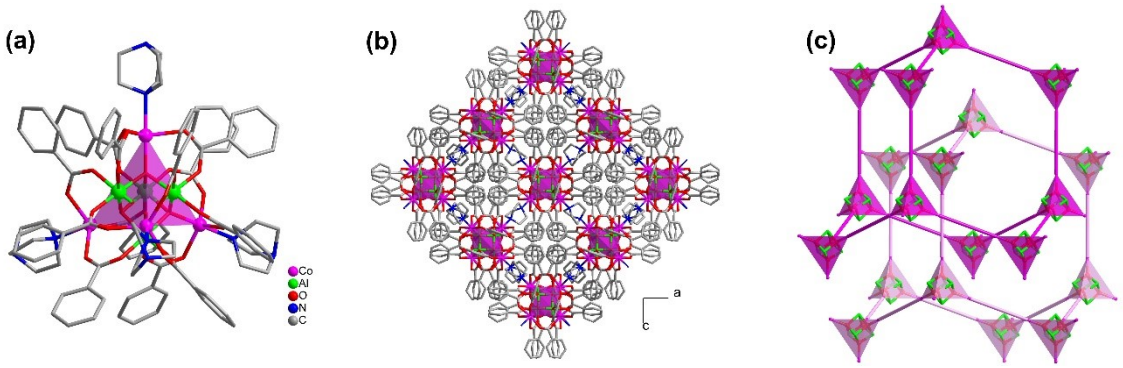

Fig. S1. (a) Structure of the heterometallic supertetrahedral cluster in **AlOC-99**; (b) 3D framework showing the arrangement of supertetrahedral clusters in **AlOC-99**; (c) The 2-fold interpenetrated structure of **AlOC-99**.

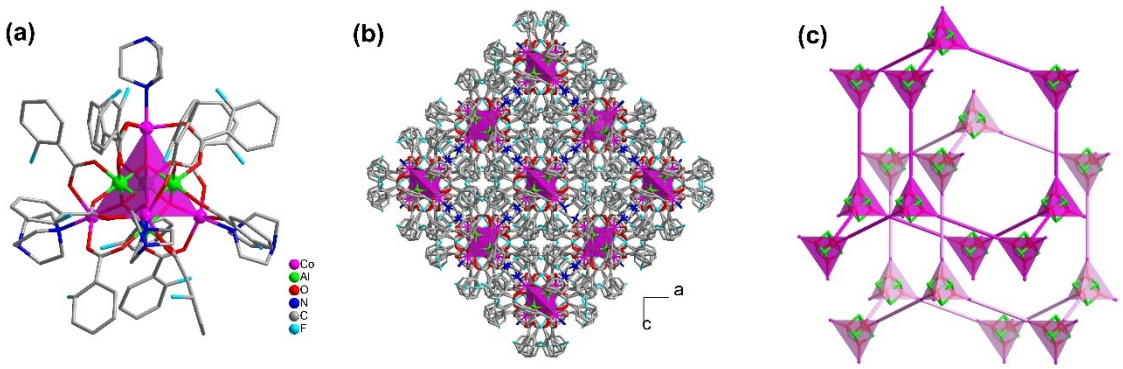

Fig. S2. (a) Structure of the heterometallic supertetrahedral cluster in **AlOC-100**; (b) 3D framework showing the arrangement of supertetrahedral clusters in **AlOC-100**; (c) The 2-fold interpenetrated structure of **AlOC-100**.

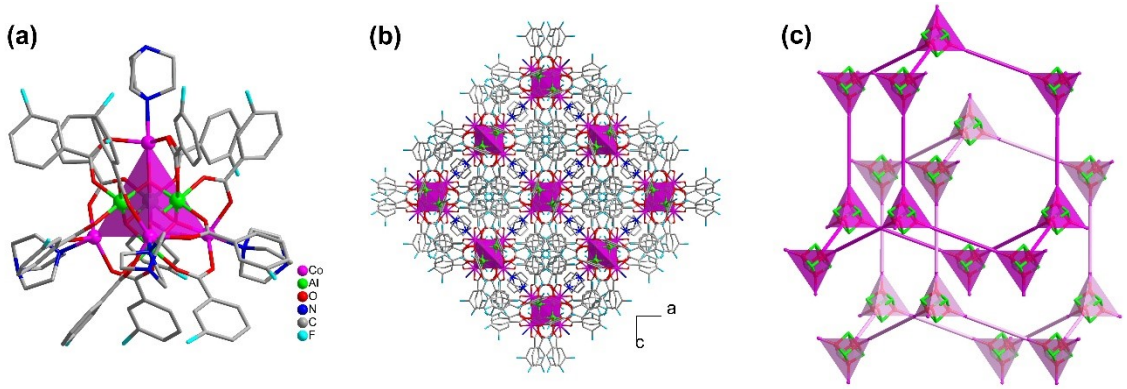

Fig. S3. (a) Structure of the heterometallic supertetrahedral cluster in **AlOC-101**; (b) 3D framework showing the arrangement of supertetrahedral clusters in **AlOC-101**; (c) The 2-fold interpenetrated structure of **AlOC-101**.

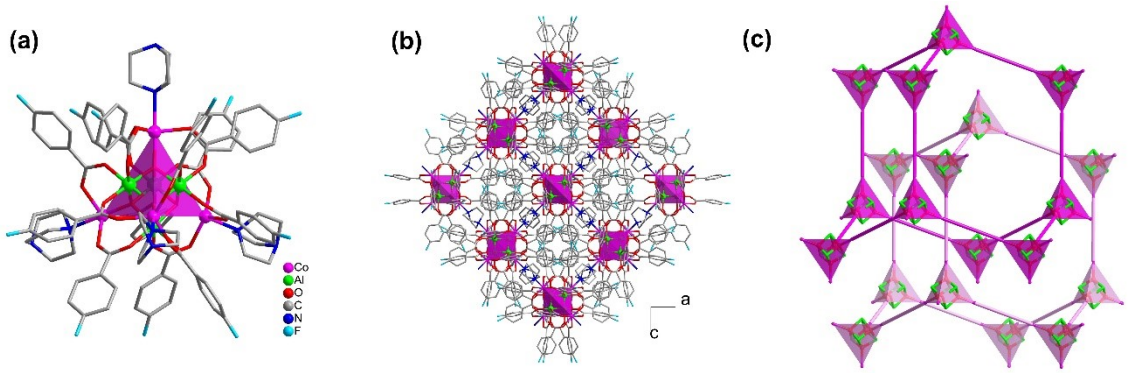

Fig. S4. (a) Structure of the heterometallic supertetrahedral cluster in **AlOC-102**; (b) 3D framework showing the arrangement of supertetrahedral clusters in **AlOC-102**; (c) The 2-fold interpenetrated structure of **AlOC-102**.

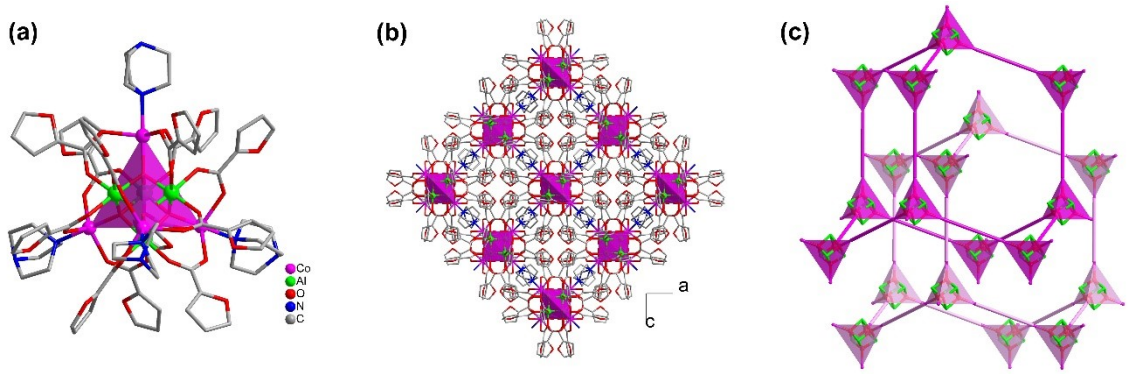

Fig. S5. (a) Structure of the heterometallic supertetrahedral cluster in **AlOC-103**; (b) 3D framework showing the arrangement of supertetrahedral clusters in **AlOC-103**; (c) The 2-fold interpenetrated structure of **AlOC-103**.

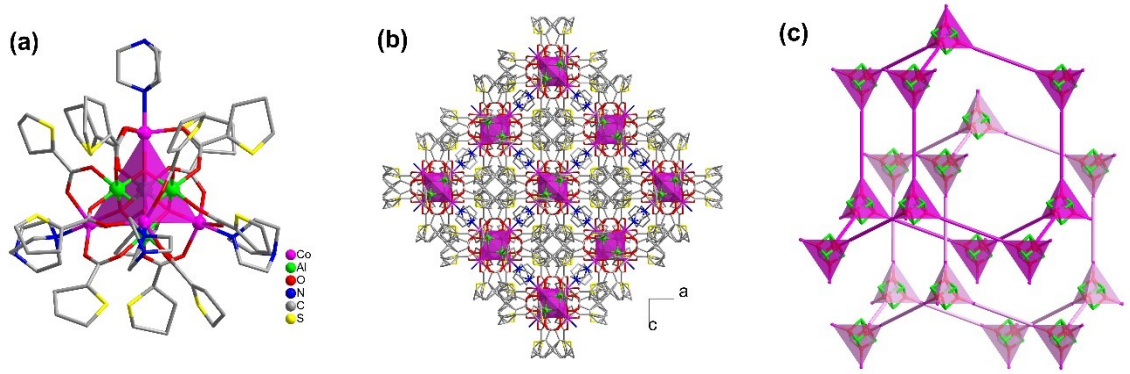

Fig. S6. (a) Structure of the heterometallic supertetrahedral cluster in **AlOC-104**; (b) 3D framework showing the arrangement of supertetrahedral clusters in **AlOC-104**; (c) The 2-fold interpenetrated structure of **AlOC-104**.

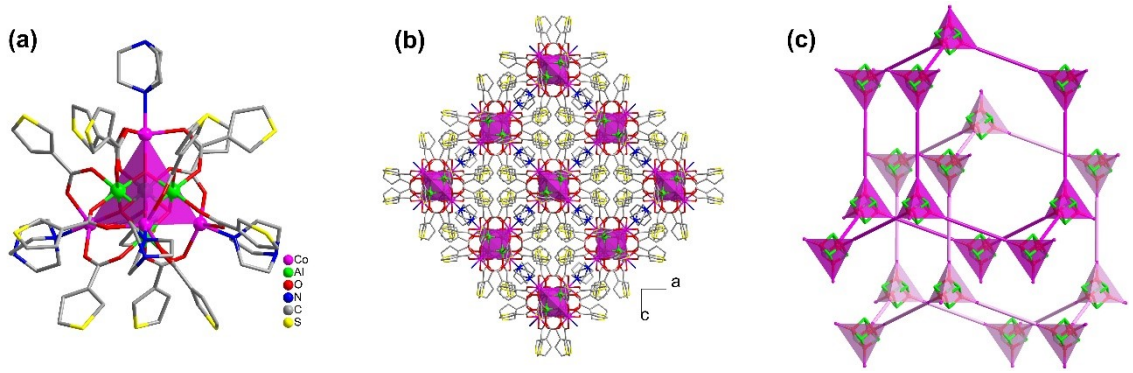

Fig. S7. (a) Structure of the heterometallic supertetrahedral cluster in **AlOC-105**; (b) 3D framework showing the arrangement of supertetrahedral clusters in **AlOC-105**; (c) The 2-fold interpenetrated structure of **AlOC-105**.

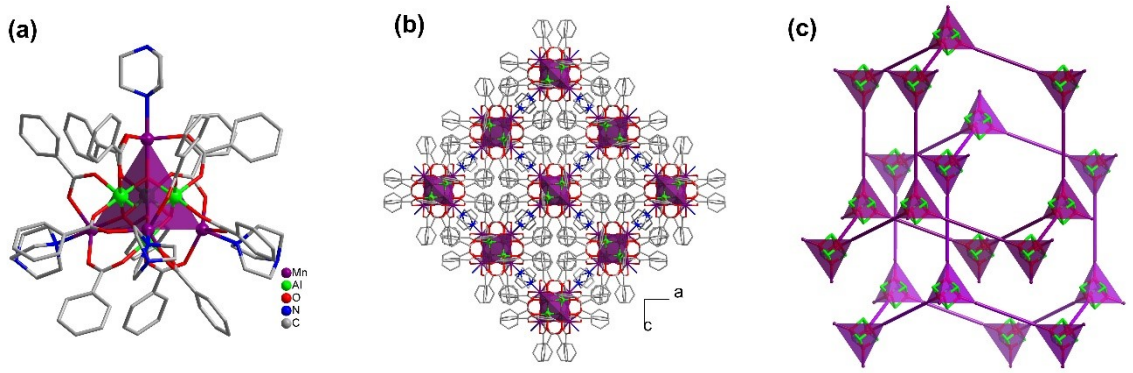

Fig. S8. (a) Structure of the heterometallic supertetrahedral cluster in **AlOC-106**; (b) 3D framework showing the arrangement of supertetrahedral clusters in **AlOC-106**; (c) The 2-fold interpenetrated structure of **AlOC-106**.

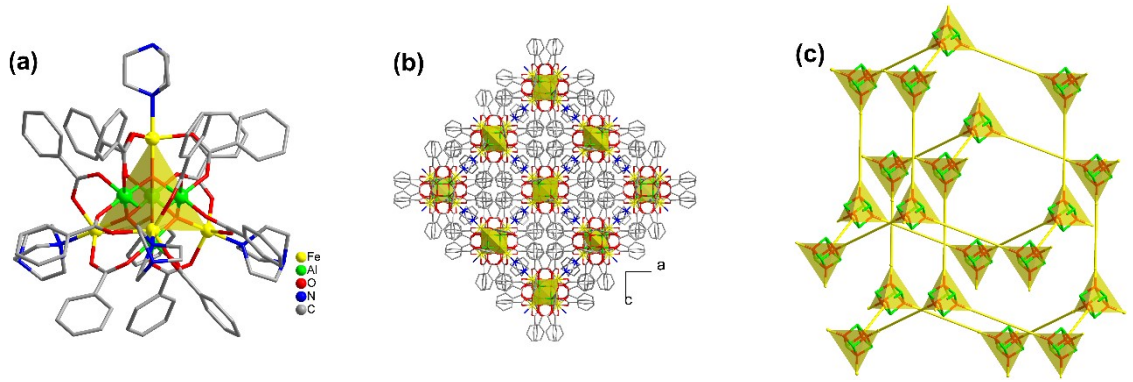

Fig. S9. (a) Structure of the heterometallic supertetrahedral cluster in **AlOC-107**; (b) 3D framework showing the arrangement of supertetrahedral clusters in **AlOC-107**; (c) The 2-fold interpenetrated structure of **AlOC-107**.

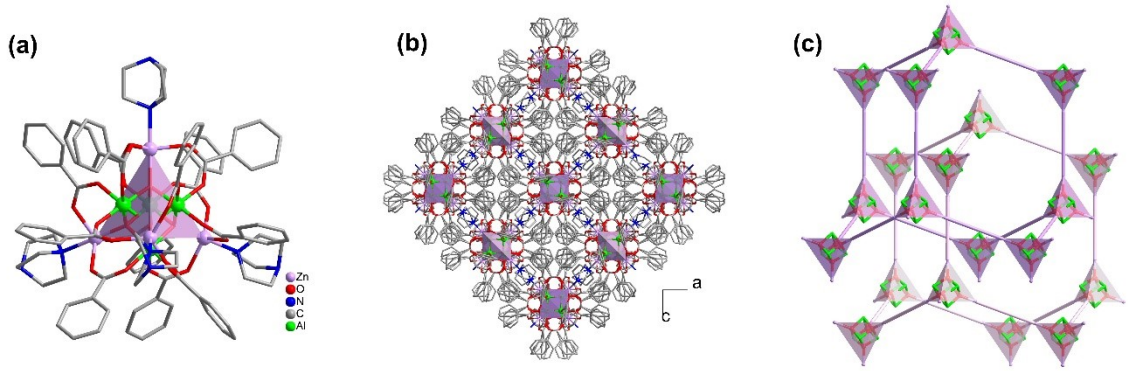

Fig. S10. (a) Structure of the heterometallic supertetrahedral cluster in **AlOC-108**; (b) 3D framework showing the arrangement of supertetrahedral clusters in **AlOC-108**; (c) The 2-fold interpenetrated structure of **AlOC-108**.

2. The supertetrahedral clusters and non-interpenetrated frameworks in AlOC-109 to AlOC-111.

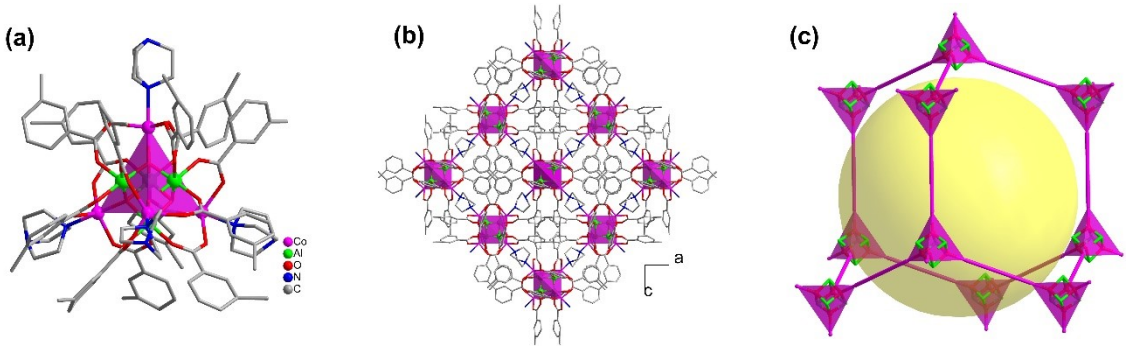

Fig. S11. (a) Structure of the heterometallic supertetrahedral cluster in **AlOC-109**; (b) 3D framework showing the arrangement of supertetrahedral clusters in **AlOC-109**; (c) The non-interpenetrated structure of **AlOC-109**.

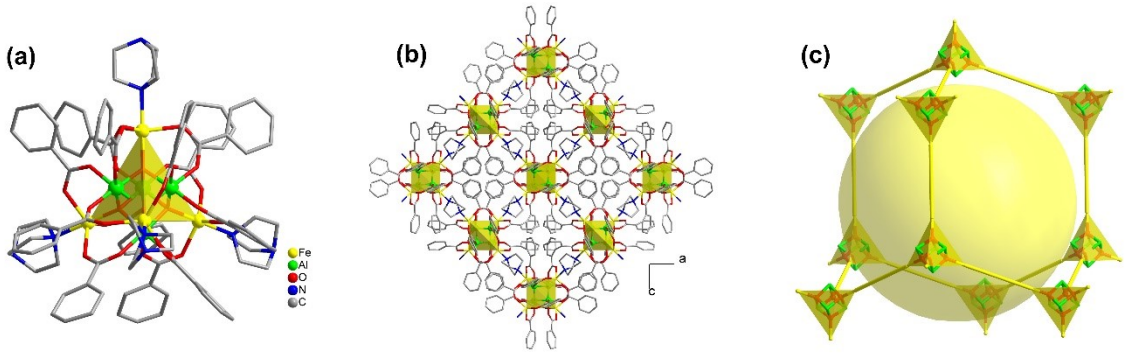

Fig. S12. (a) Structure of the heterometallic supertetrahedral cluster in **AlOC-110**; (b) 3D framework showing the arrangement of supertetrahedral clusters in **AlOC-110**; (c) The non-interpenetrated structure of **AlOC-110**.

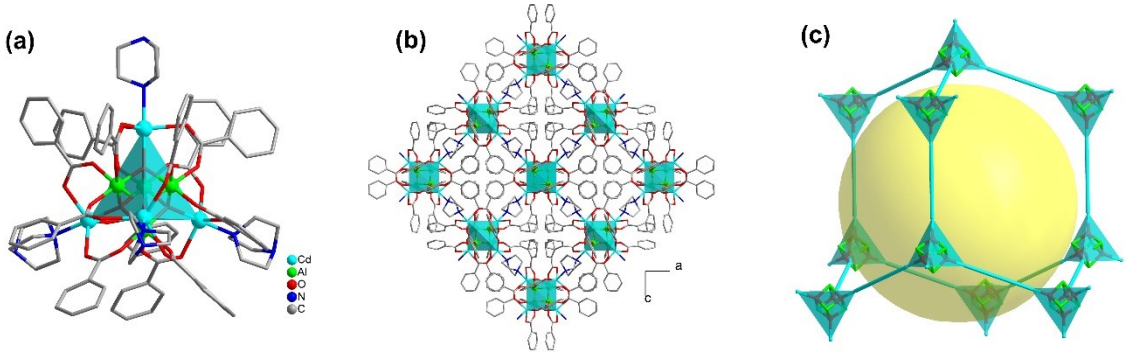

Fig. S13. (a) Structure of the heterometallic supertetrahedral cluster in **AlOC-111**; (b) 3D framework showing the arrangement of supertetrahedral clusters in **AlOC-111**; (c) The non-interpenetrated structure of **AlOC-111**.

3. The supertetrahedral clusters and lonsdaleite *(lon)* frameworks in AlOC-112 to AlOC-120.

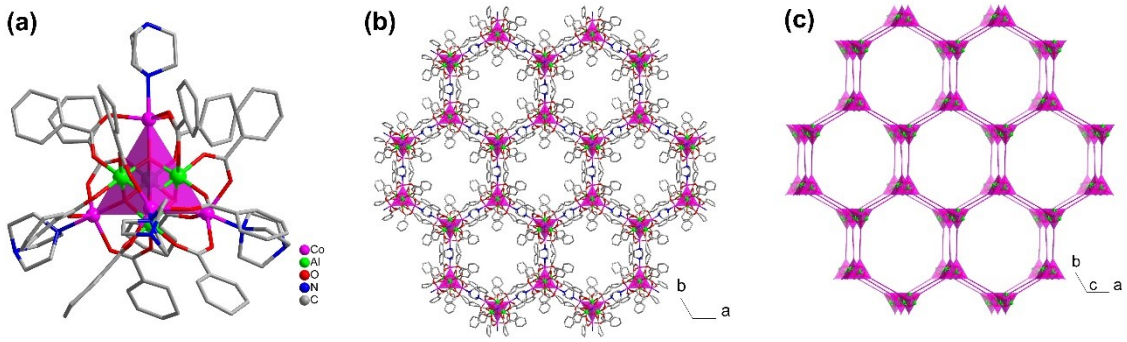

Fig. S14. (a) Structure of the heterometallic supertetrahedral cluster in **AlOC-112**; (b) 3D framework showing the arrangement of supertetrahedral clusters in **AlOC-112**; (c) The non-interpenetrated 3D topological structure of **AlOC-112**.

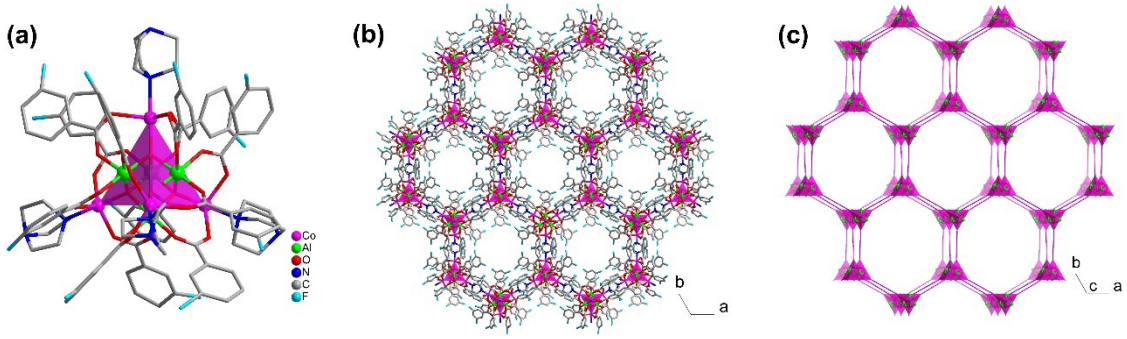

Fig. S15. (a) Structure of the heterometallic supertetrahedral cluster in **AlOC-113**; (b) 3D framework showing the arrangement of supertetrahedral clusters in **AlOC-113**; (c) The non-interpenetrated 3D topological structure of **AlOC-113**.

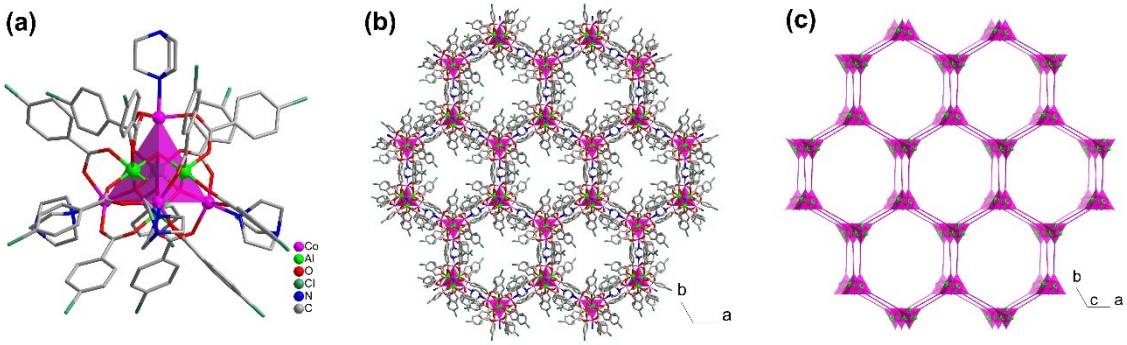

Fig. S16. (a) Structure of the heterometallic supertetrahedral cluster in **AlOC-114**; (b) 3D framework showing the arrangement of supertetrahedral clusters in **AlOC-114**; (c) The non-interpenetrated 3D topological structure of **AlOC-114**.

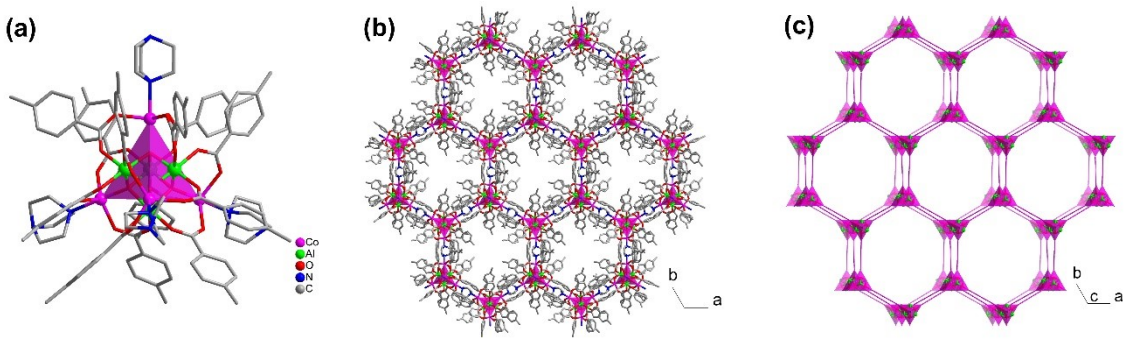

Fig. S17. (a) Structure of the heterometallic supertetrahedral cluster in **AlOC-115**; (b) 3D framework showing the arrangement of supertetrahedral clusters in **AlOC-115**; (c) The non-interpenetrated 3D topological structure of **AlOC-115**.

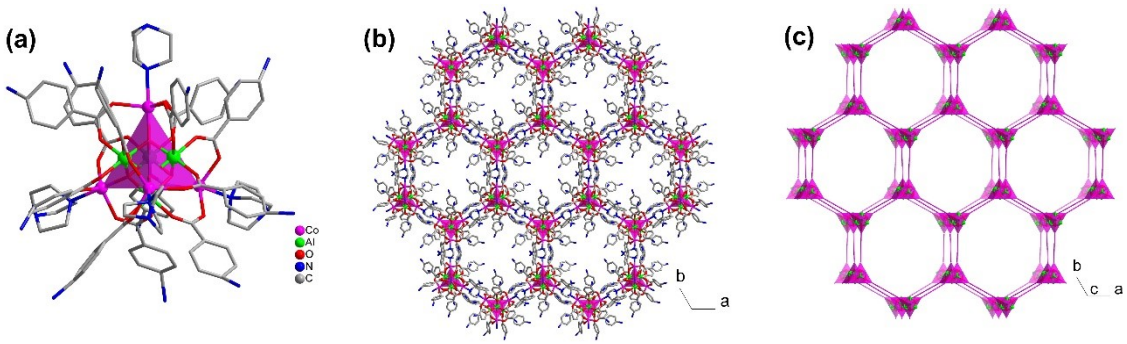

Fig. S18. (a) Structure of the heterometallic supertetrahedral cluster in **AlOC-116**; (b) 3D framework showing the arrangement of supertetrahedral clusters in **AlOC-116**; (c) The non-interpenetrated 3D topological structure of **AlOC-116**.

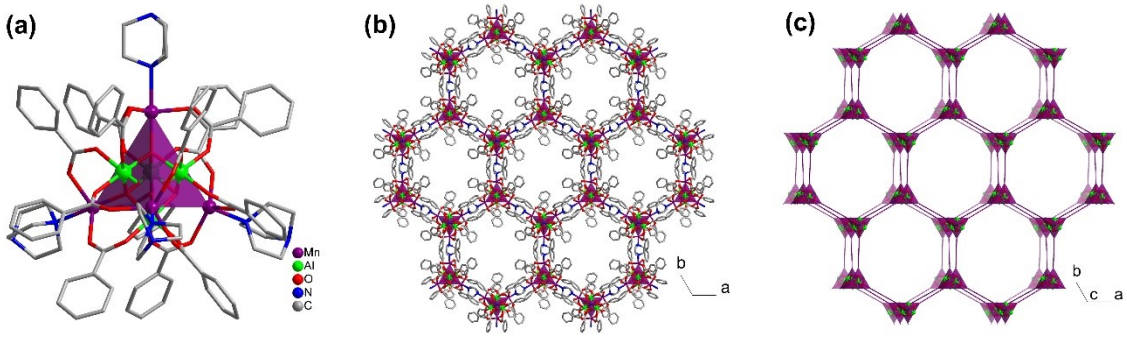

Fig. S19. (a) Structure of the heterometallic supertetrahedral cluster in **AlOC-117**; (b) 3D framework showing the arrangement of supertetrahedral clusters in **AlOC-117**; (c) The non-interpenetrated 3D topological structure of **AlOC-117**.

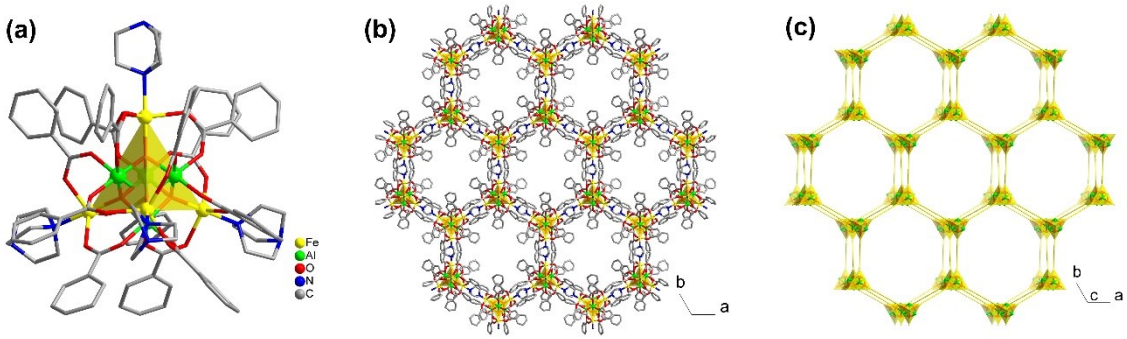

Fig. S20. (a) Structure of the heterometallic supertetrahedral cluster in **AlOC-118**; (b) 3D framework showing the arrangement of supertetrahedral clusters in **AlOC-118**; (c) The non-interpenetrated 3D topological structure of **AlOC-118**.

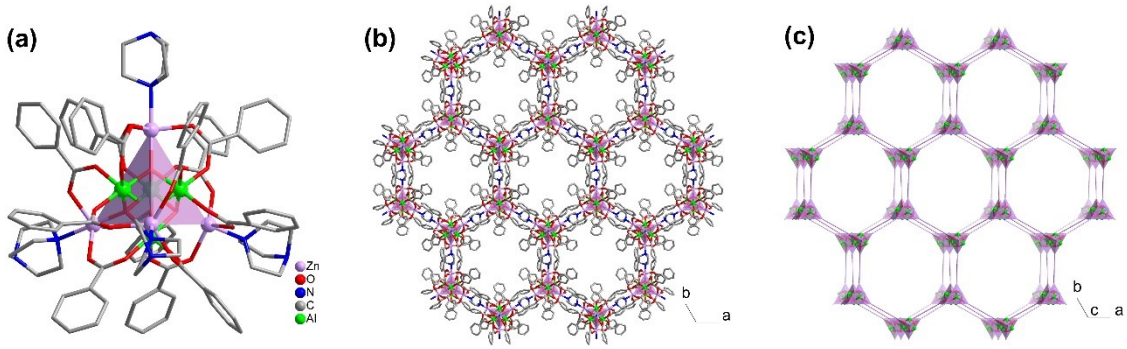

Fig. S21. (a) Structure of the heterometallic supertetrahedral cluster in **AlOC-119**; (b) 3D framework showing the arrangement of supertetrahedral clusters in **AlOC-119**; (c) The non-interpenetrated 3D topological structure of **AlOC-119**.

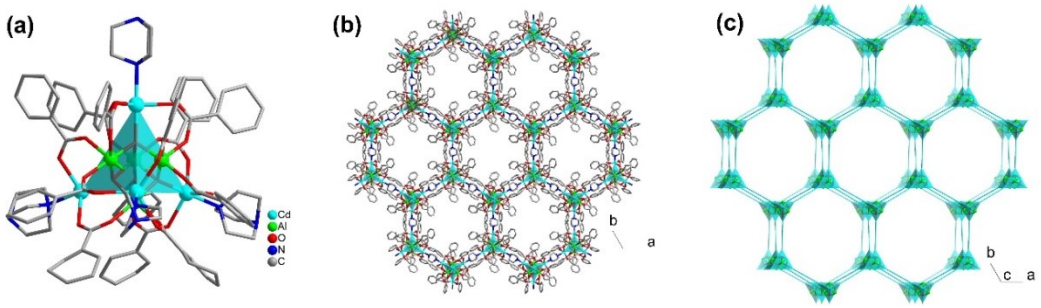

Fig. S22. (a) Structure of the heterometallic supertetrahedral cluster in **AlOC-120**; (b) 3D framework showing the arrangement of supertetrahedral clusters in **AlOC-120**; (c) The non-interpenetrated 3D topological structure of **AlOC-120**.

4. The detail coordination environment information for Al ion, Co ion and ligands in AlOC-99.

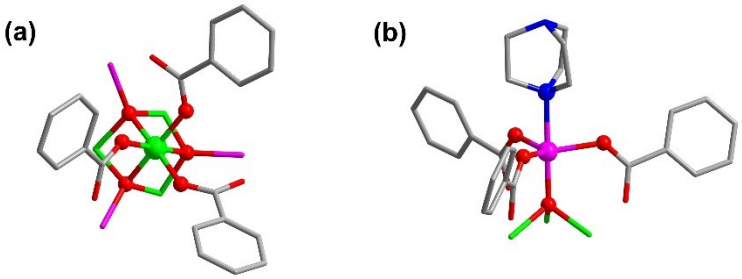

Fig. S23. The coordination environments of Al (a) and Co (b) ions. Colour code: Al green; Co pink; N blue; O red; C grey. H atoms are omitted for clarity.

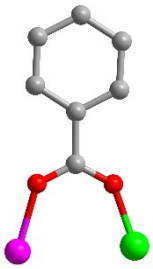

Fig. S24. The coordination mode of benzoate. Colour code: Al green; Co pink; O red; C grey. H atoms are omitted for clarity.

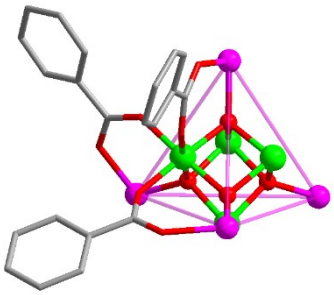

Fig. S25. The face-capping view of the supertetrahedral cluster. Colour code: Al green; Co pink; O red; C grey. H atoms are omitted for clarity.

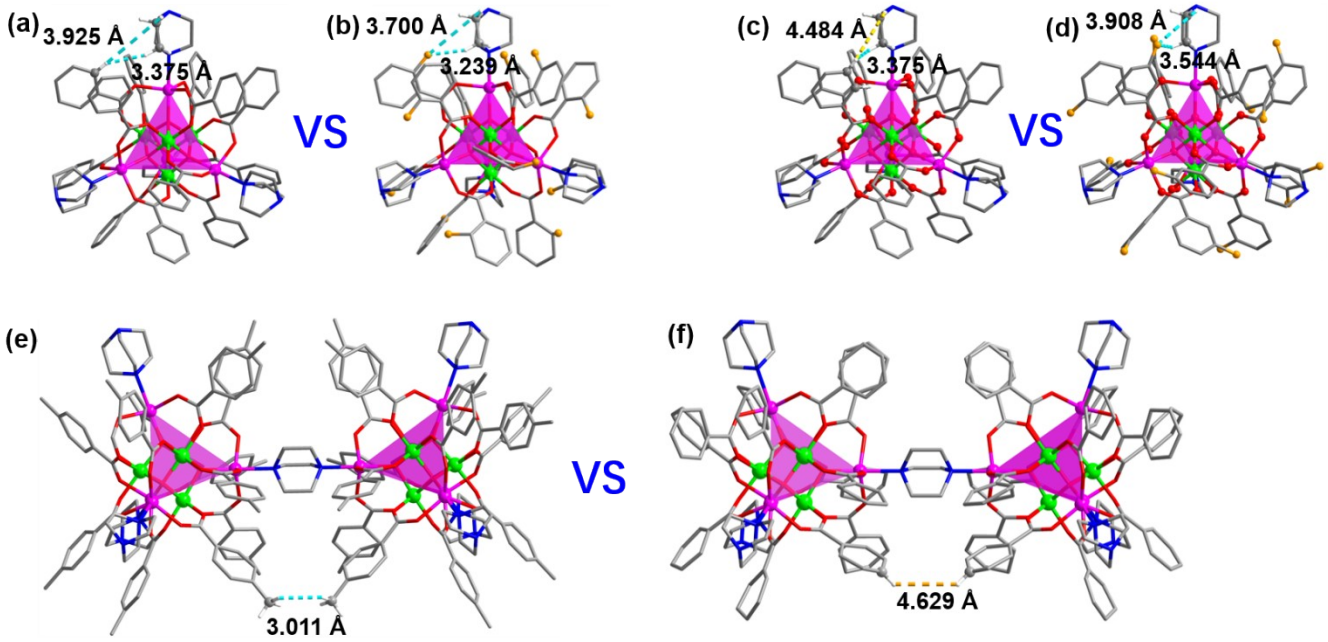

Fig. S26. The comparison of hydrogen bonds in different chelated ligands modified frameworks. (a) and (b) The hydrogen bond positions and lengths in **AlOC-99** (a) and **AlOC-100** (b); (c) and (d) the hydrogen bond positions and lengths in **AlOC-99** (c) and **AlOC-101** (d), the dotted yellow line indicates that the bond length is too long to form hydrogen bond in **AlOC-99**; (e) and (f) the hydrogen bond positions and lengths in **AlOC-115** (e) and **AlOC-112** (f), the dotted yellow line indicates that the bond length is too long to form hydrogen bond in **AlOC-112**. Colour code: Al green; Co pink; O red; C grey; F orange. H atoms are omitted for clarity.

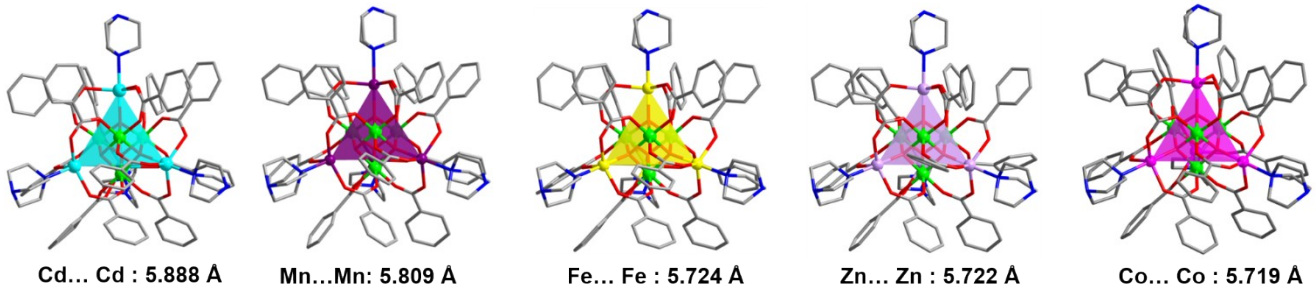

Fig. S27. The size of the different supertetrahedral cluster. Colour code: Al green; Cd turquoise; Mn violet; Fe yellow; Zn lavender; Co pink; O red; C grey. H atoms are omitted for clarity.

5. The packing of supertetrahedral cluster in AlOC-112.

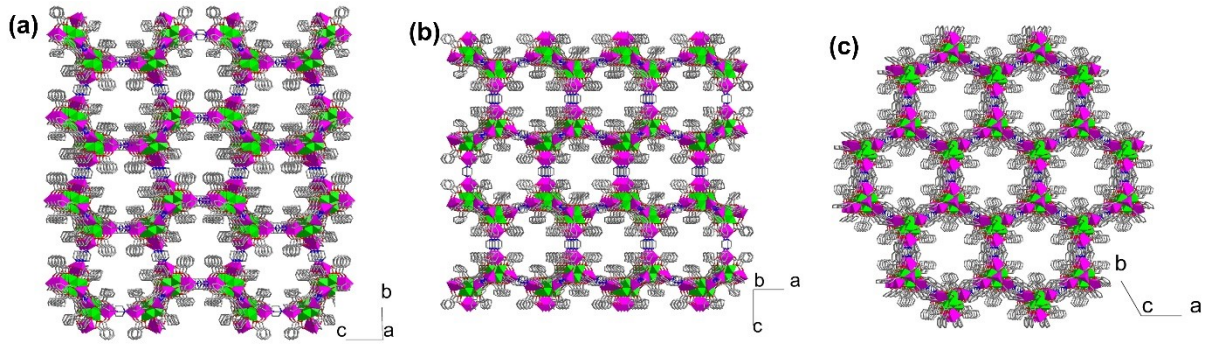

Fig. S28. View of the 3D frameworks of **AlOC-112** along the a axis (a), b axis (b) and c axis (c).

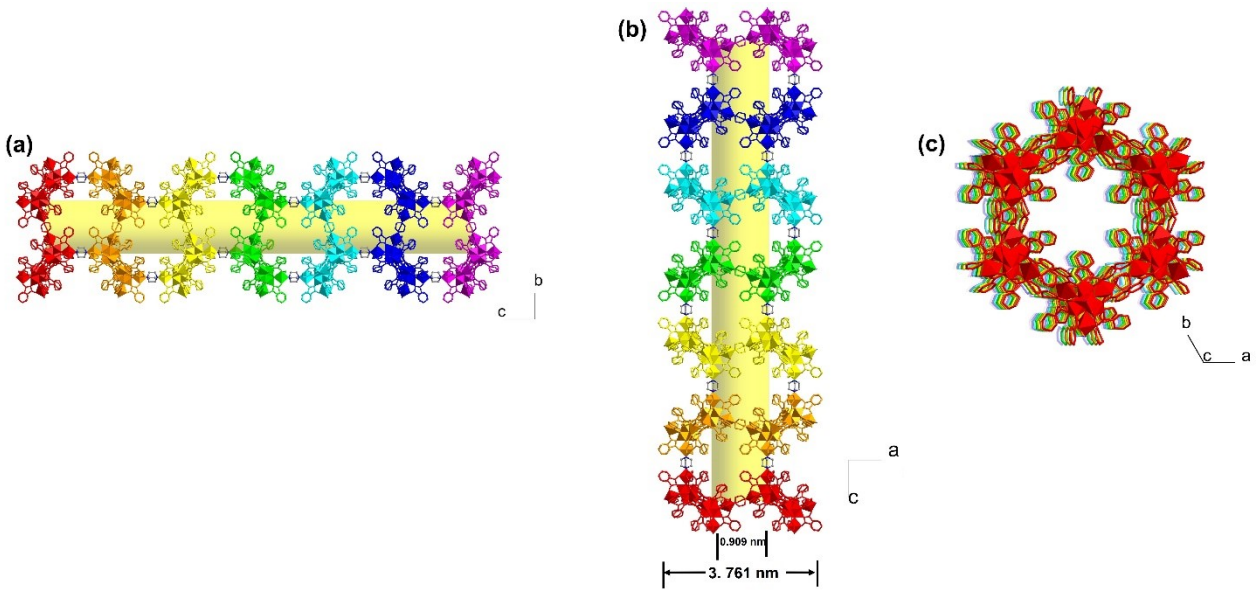

Fig. S29. The view of 1D nanotubes along the a axis (a), b axis (b) and c axis (c).

6. The mesoporous cavity in non-interpenetrated diamond (*dia*) frameworks.

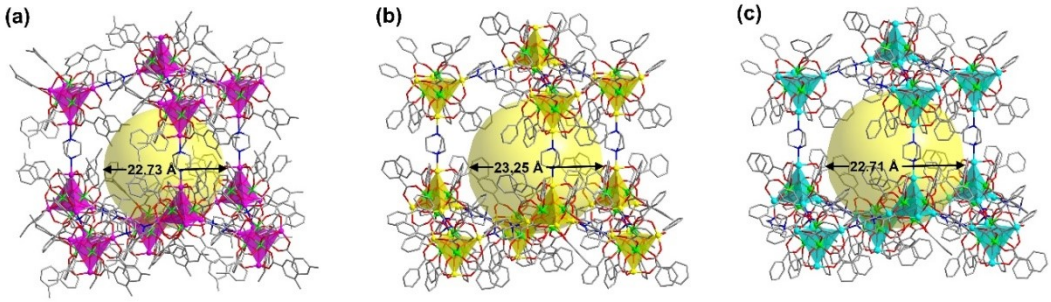

Fig. S30. The diamond (***dia***) cavity in **AlOC-109** (a), **AlOC-110** (b) and **AlOC-111** (c).

7. The N_2 and CO_2 sorption isotherms of AlOC-99, AlOC-109 and AlOC-112.

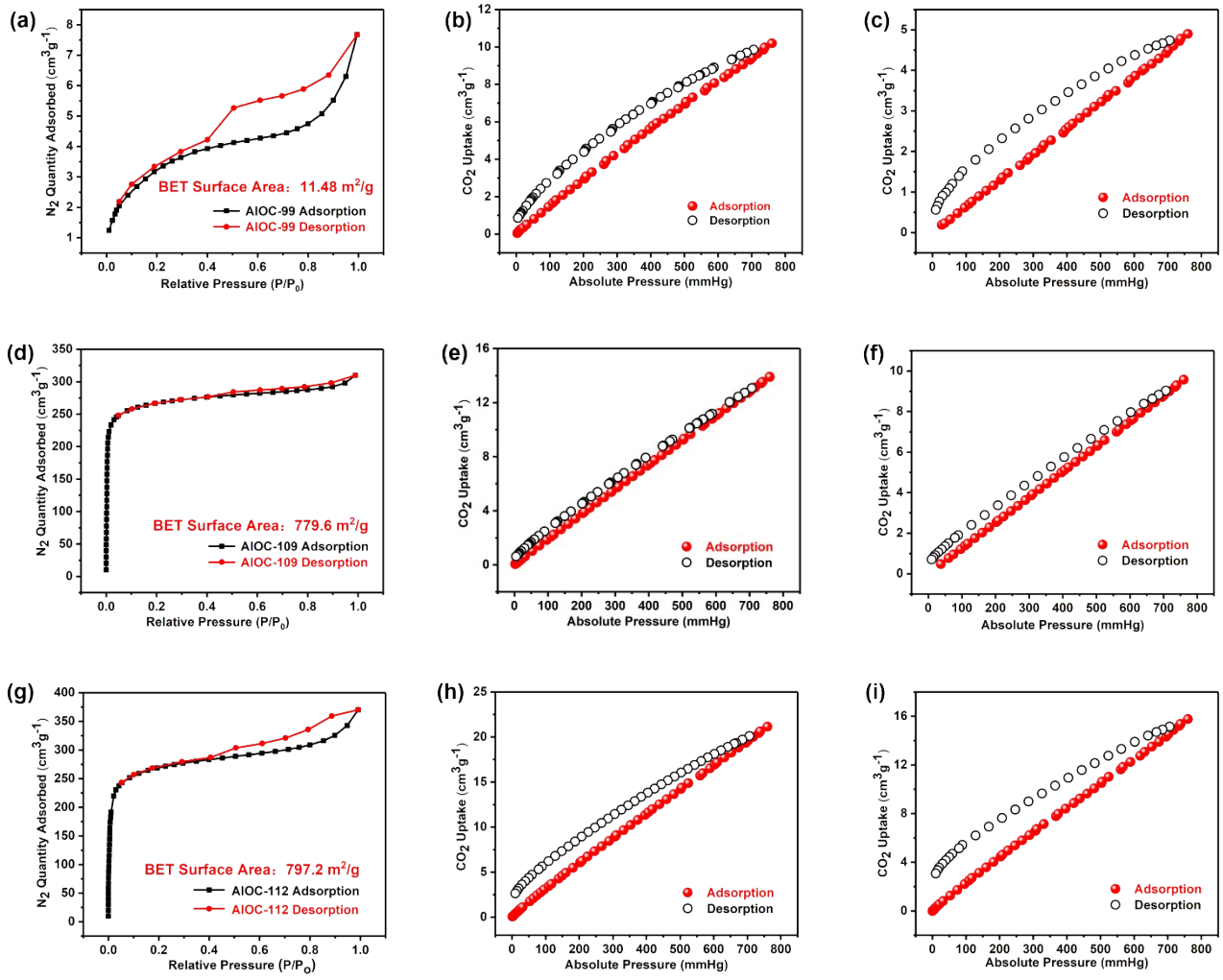

Fig. S31. (a) N_2 sorption isotherms of **AlOC-99** at 77K; (b) CO_2 sorption isotherms of **AlOC-99** at 273K; (c) CO_2 sorption isotherms of **AlOC-99** at 298K; (d) N_2 sorption isotherms of **AlOC-109** at 77K; (e) CO_2 sorption isotherms of **AlOC-109** at 273K; (f) CO_2 sorption isotherms of **AlOC-109** at 298K; (g) N_2 sorption isotherms of **AlOC-112** at 77K; (h) CO_2 sorption isotherms of **AlOC-112** at 273K; (i) CO_2 sorption isotherms of **AlOC-112** at 298K.

8. The stabilities and hydrophobic properties of AlOC-99, AlOC-109 and AlOC-112.

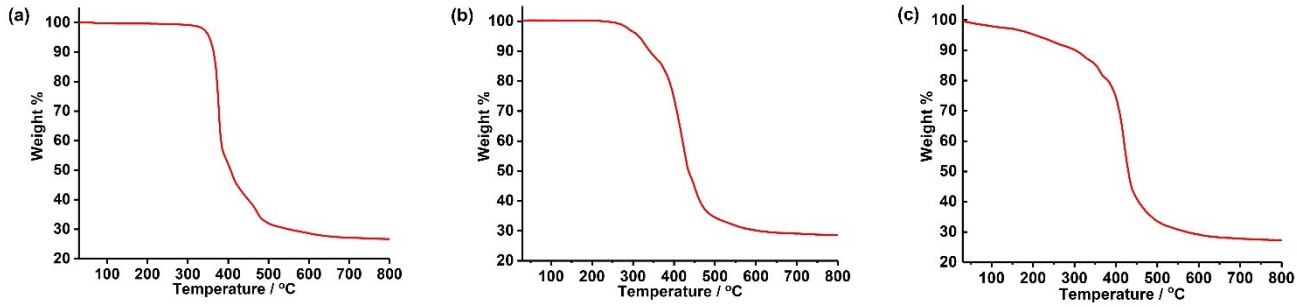

Fig. S32. The TGA curves of **AlOC-99** (a), **AlOC-109** (b) and **AlOC-112** (c) measured in N_2/O_2 from room temperature to 800 °C.

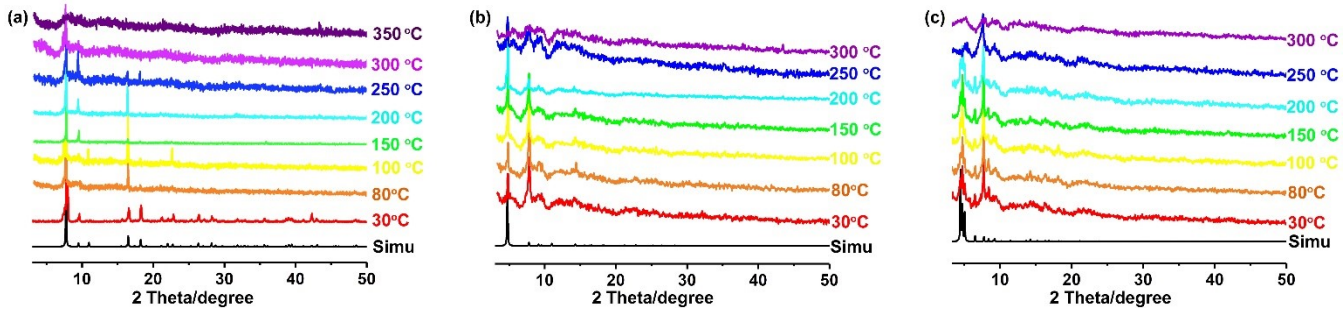

Fig. S33. In-situ temperature-dependent PXRD patterns for **AlOC-99** (a), **AlOC-109** (b) and **AlOC-112** (c).

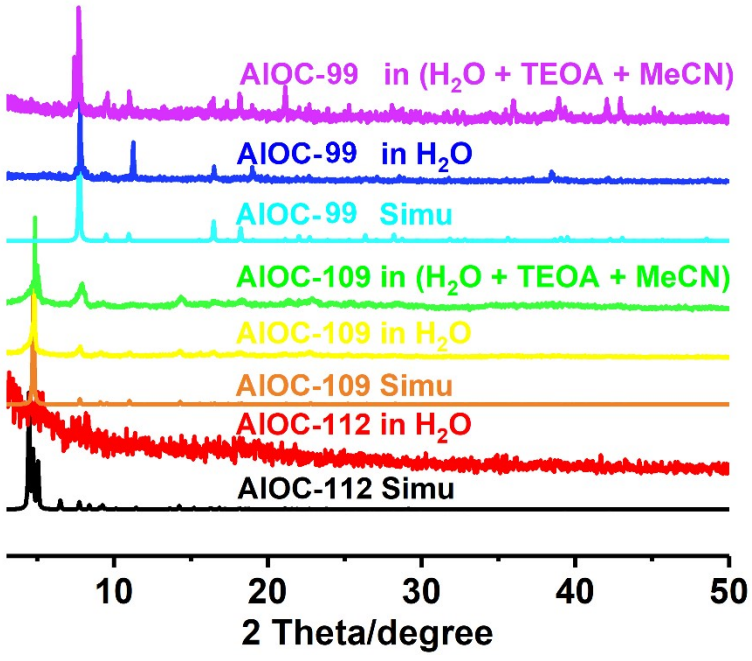

Fig. S34. The PXRD patterns of **AlOC-99**, **AlOC-109** and **AlOC-112** after immersing in H_2O or TEOA solution.

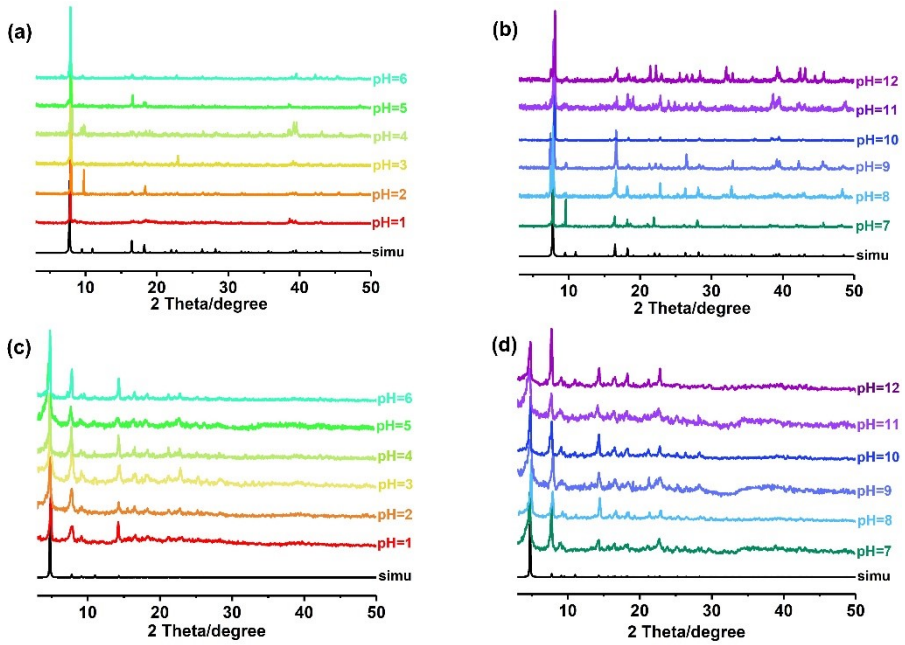

Fig. S35. The PXRD patterns of **AlOC-99** (a and b) and **AlOC-109** (c and d) after soaking in aqueous solution with different pH value for 24h.

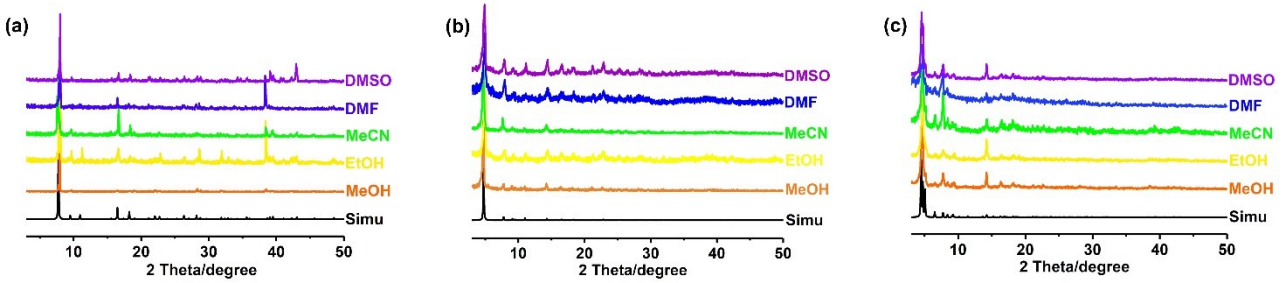

Fig. S36. The PXRD patterns of **AlOC-99** (a), **AlOC-109** (b) and **AlOC-112** (c) after soaking in different organic solvents at room temperature for 24h.

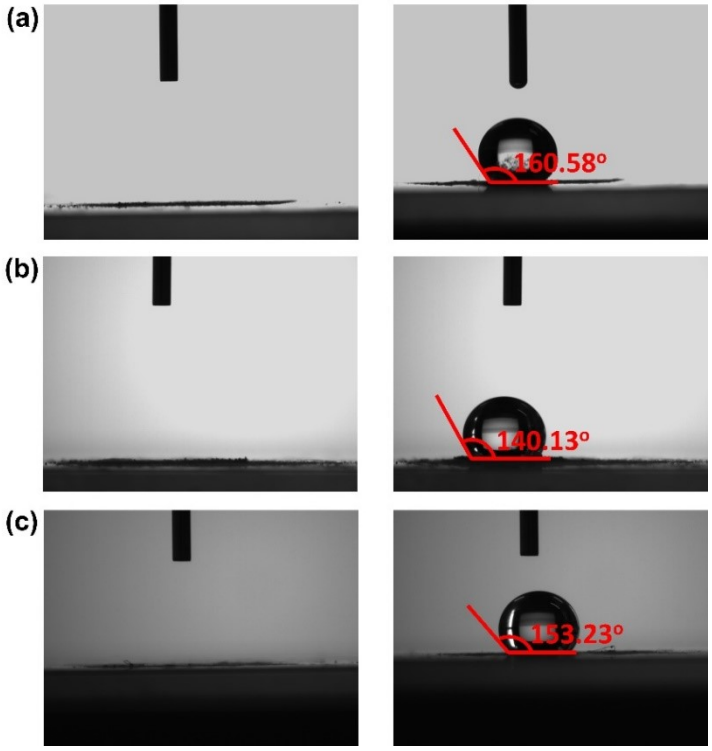

Fig. S37. The contact angle measurements of **AlOC-99** (a), **AlOC-109** (b) and **AlOC-112** (c).

Fig. S38. The digital photo of **AlOC-99** floating on the water. Although the density of **AlOC-99** is large than water, the crystals can still float on surface of water indicating there are strong surface tension and interface hydrophobic.

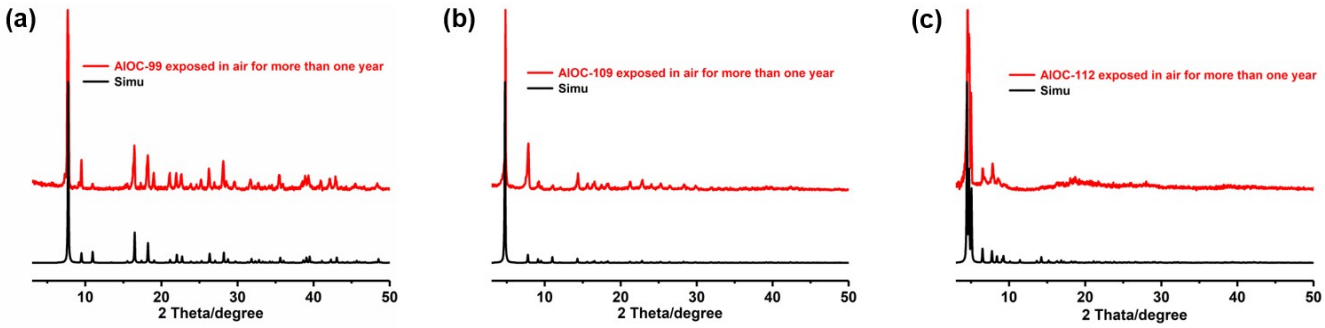

Fig. S39. The PXRD patterns of **AlOC-99**, **AlOC-109** and **AlOC-112** after exposed in air for more than one year.

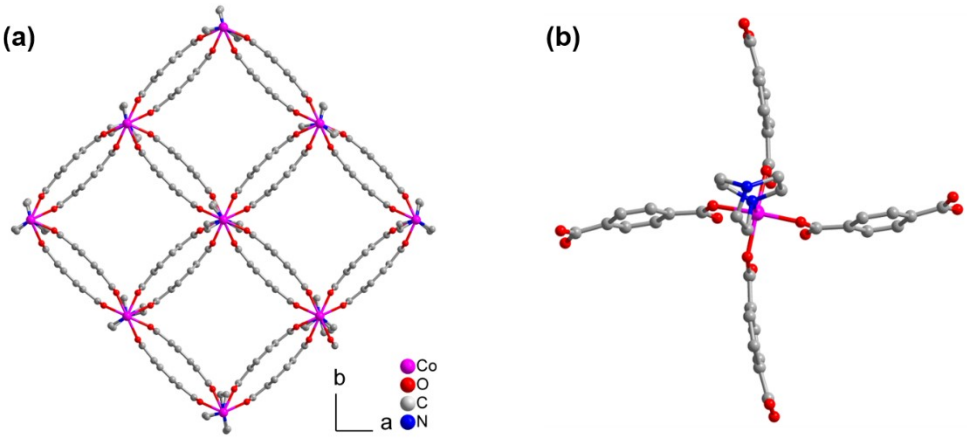

Fig. S40. The structure of Co_2Bdc_2Dabco (a) reported in literature and the coordination environment of Co in Co_2Bdc_2Dabco (b).

9. PXRD analyses.

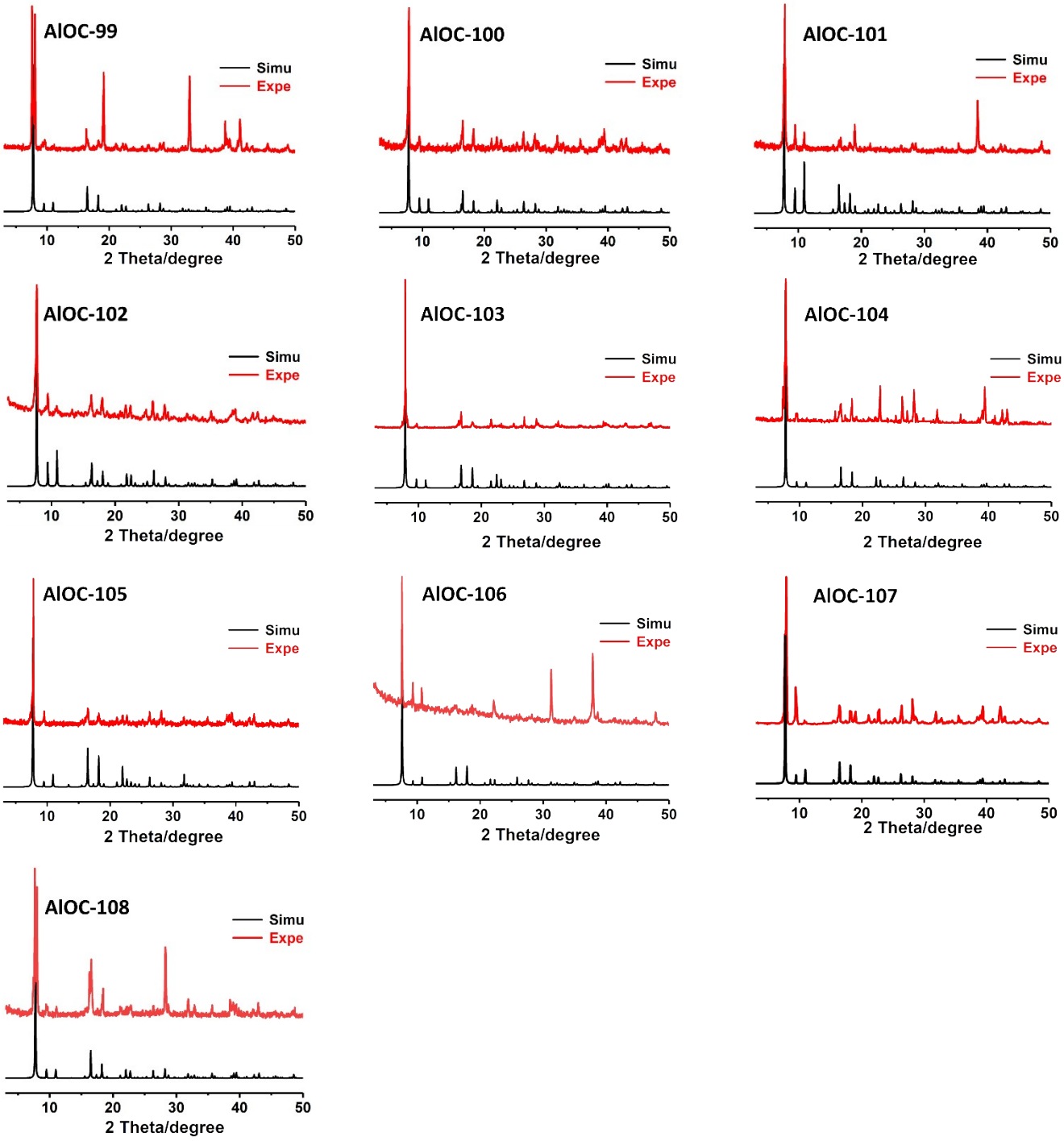

Fig. S41. The PXRD patterns of two-fold interpenetrated diamond (***dia***) frameworks (simulated, black; experimental, red).

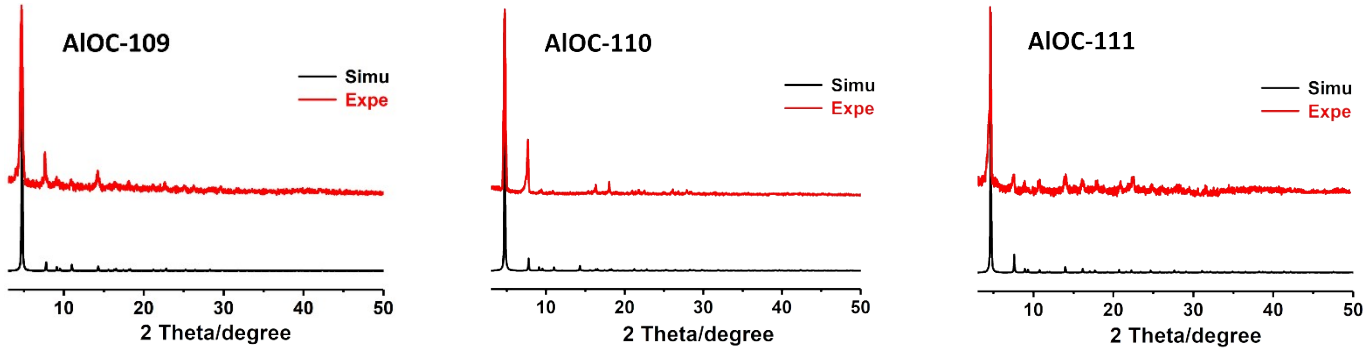

Fig. S42. The PXRD patterns of non-interpenetrated diamond (***dia***) frameworks (simulated, black; experimental, red).

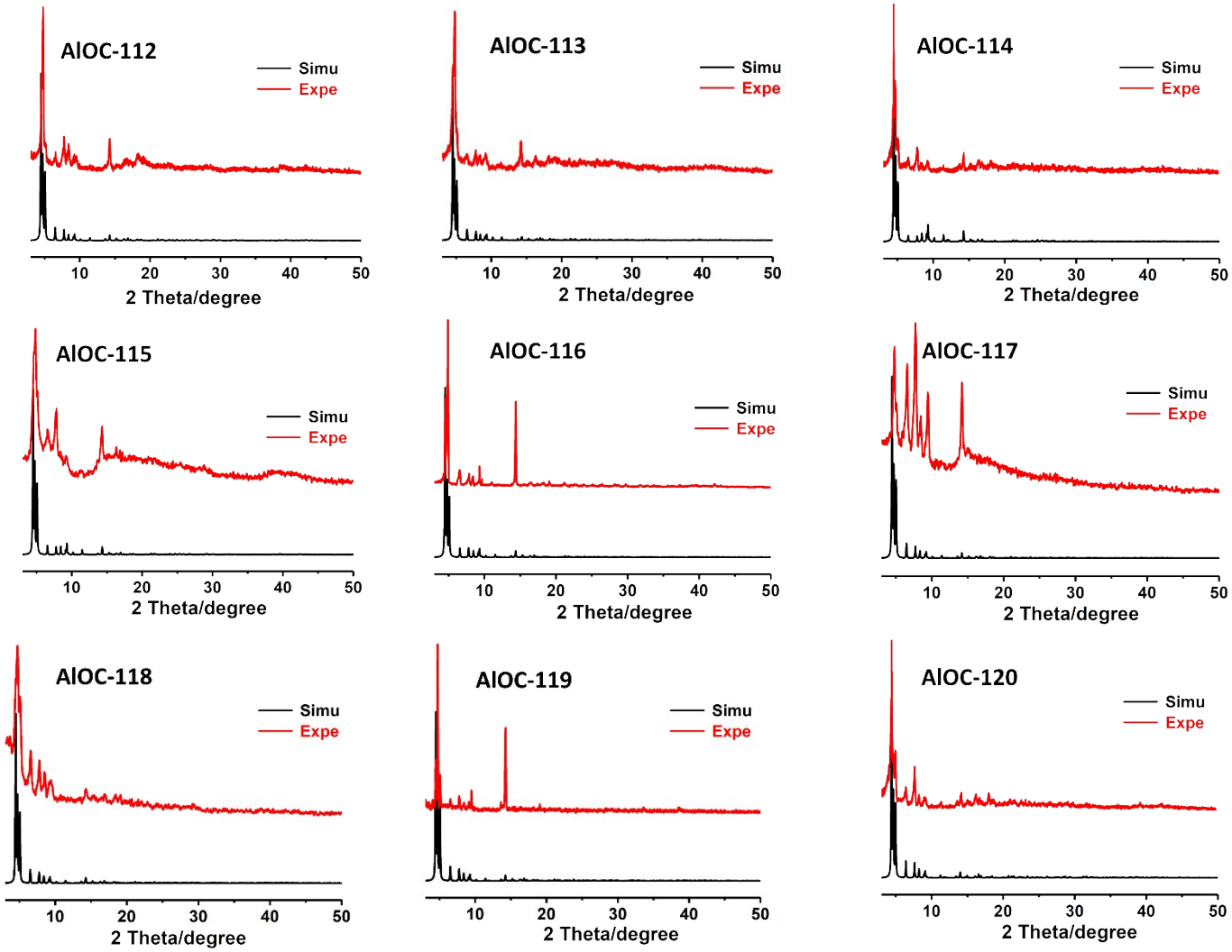

Fig. S43. The PXRD patterns of non-interpenetrated lonsdaleite ***(lon)*** frameworks (simulated, black; experimental, red).

Discussion for PXRD patterns:

The experimental PXRD patterns for **AlOC-99** to **AlOC-120** are consistent with the simulated ones from single-crytsal X-ray diffraction, which indicates that the samples are pure (Fig. S41–S43). The differences in indendity between the experimental and simulated patterns might be due to the variation in crystal orientation for power samples.

10. FT-IR spectra.

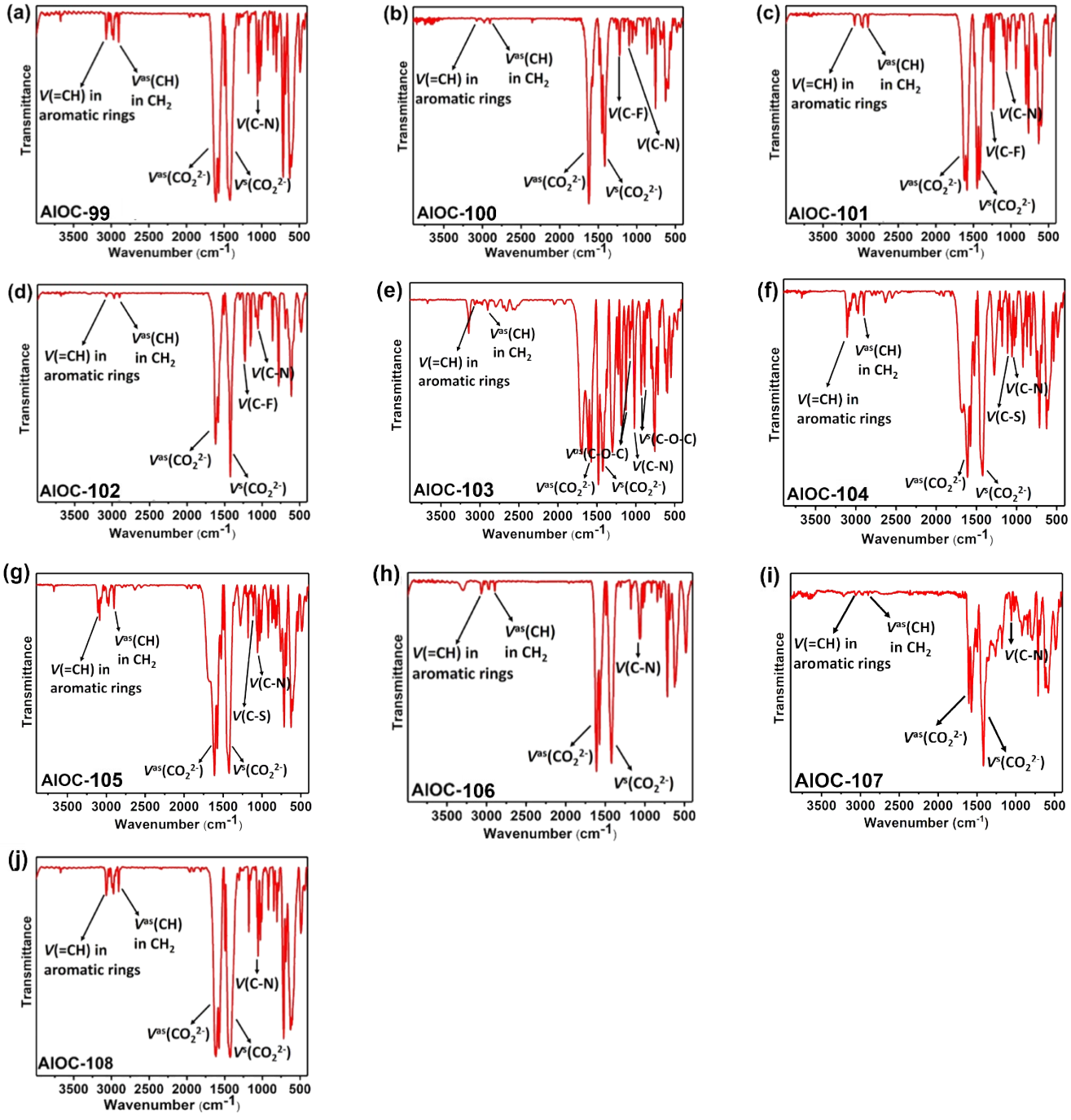

Fig. S44. The IR spectra of two-fold interpenetrated diamond (***dia***) frameworks.

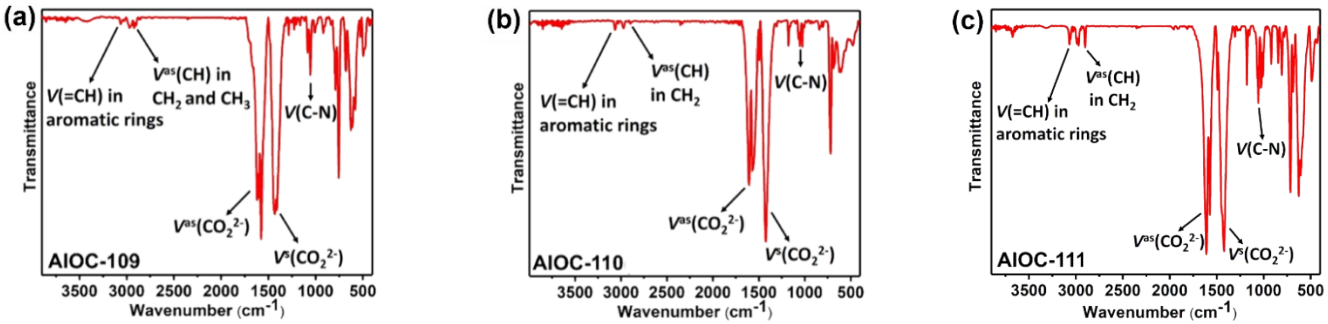

Fig. S45. The IR spectra of non-interpenetrated diamond (***dia***) frameworks.

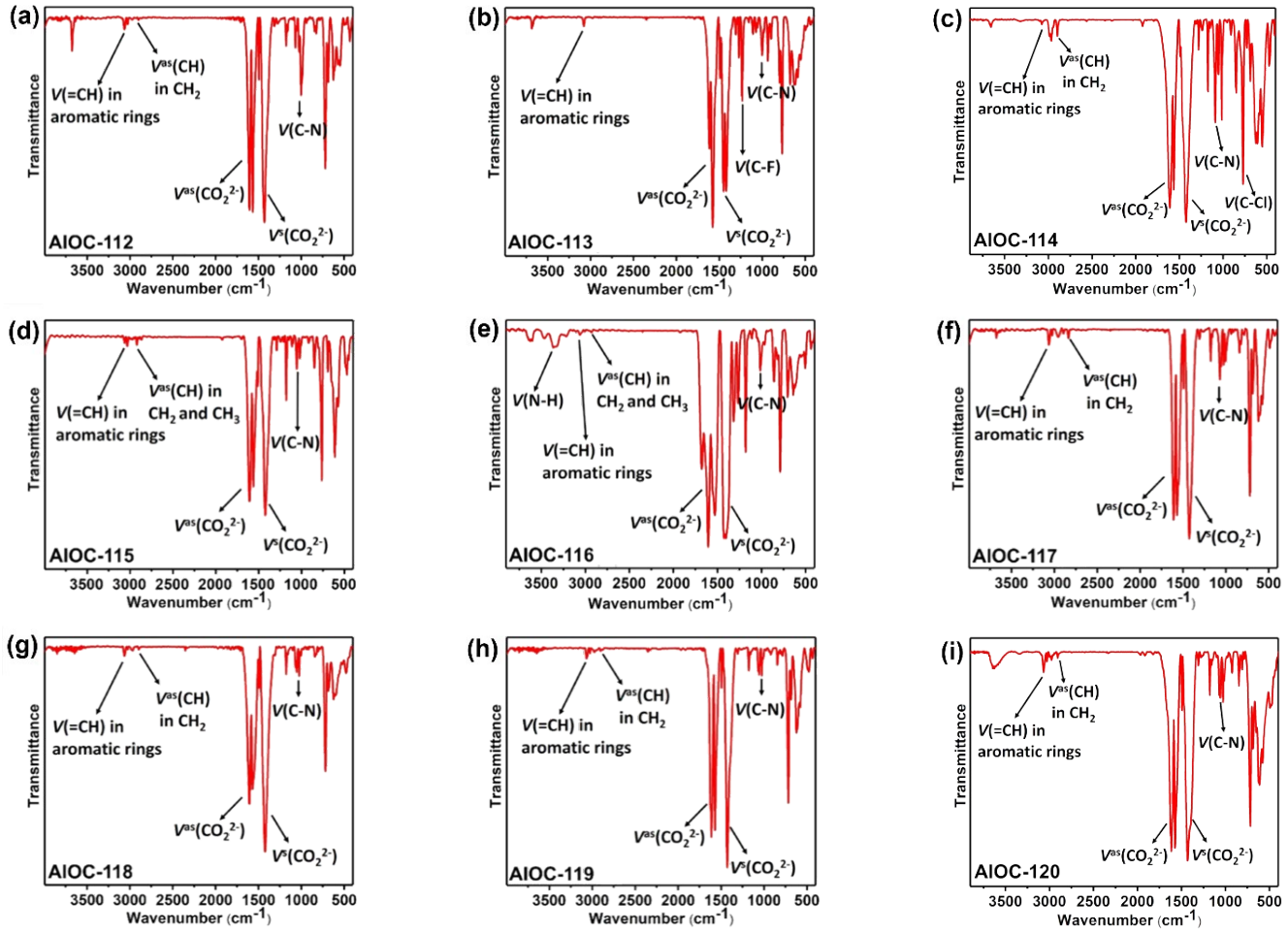

Fig. S46. The IR spectra of non-interpenetrated lonsdaleite ***(lon)*** frameworks.

Discussion for IR spectra:

The IR spectra have been recorded in the range of 3900–400 cm^{-1} from solid samples palletized with KBr, which are presented in Fig. S44–S46. In the high wavenumber region (ν > 1000 cm^{-1}), the weak absorption bands at 3097–3060 cm^{-1}, 2920–2893 cm^{-1} can be ascribed to the stretching vibration modes of C–H bonds in aromatic rings, methylene or methyl groups. The characteristic stretching vibrations $\nu(CO_2^{2-})$ of in carboxylic groups and ν(C=C) in benzene rings are overlapped from 1622 cm^{-1} to 1407 cm^{-1}. Among them, the asymmetric stretching vibration (ν_{as}) and symmetric stretching vibration (ν_s) of the carboxylate group can be clearly attributed, namely, the band at 1622−1566 cm^{-1} is assigned to the $\nu_{as}(CO_2^{2-})$ whilst the signal at 1448−1407 cm^{-1} is ascribed to the $\nu_s(CO_2^{2-})$. Besides, the intense absorption peaks appearing at 1099−1001 cm^{-1} are assigned to the stretching vibrations of ν(C−N) from DABCO. In the low wavenumber region (ν < 1000 cm^{-1}), the absorptions in the region ca. 900−650 cm^{-1} for **AlOC-99** to **AlOC-120** can be attributed to the C–H in-plane or out-of-plane bends, ring breathing, and ring deformation absorptions of benzoates.

11. The EDS spectra.

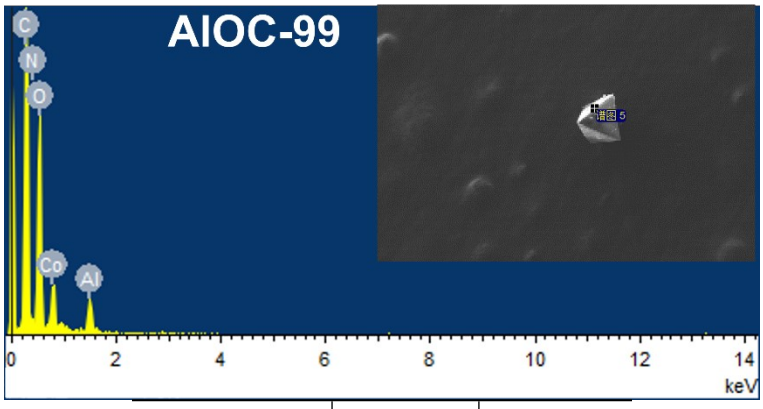

Elements	Wt. %	Mol.%
C	52.23	65.24
O	30.25	28.36
N	0.53	0.57
Co	12.01	3.06
Al	4.98	2.77

Fig. S47. The EDS spectrum and quantitative analysis of **AlOC-99**.

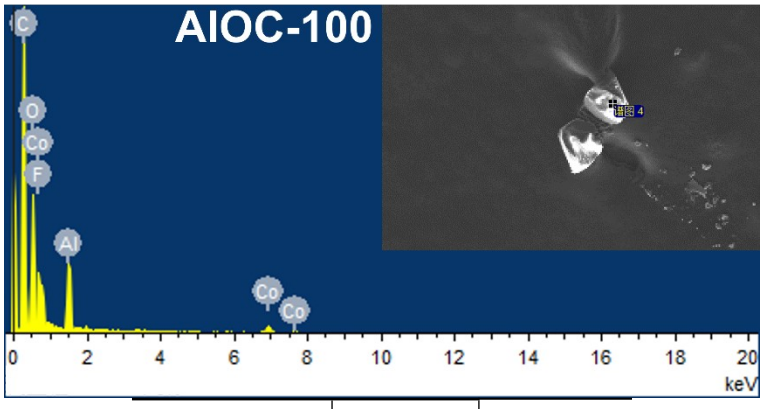

Elements	Wt. %	Mol.%
C	53.50	67.42
O	19.47	18.42
F	10.63	8.47
Co	11.38	2.87

Al	5.02	2.82

Fig. S48. The EDS spectrum and quantitative analysis of **AlOC-100**.

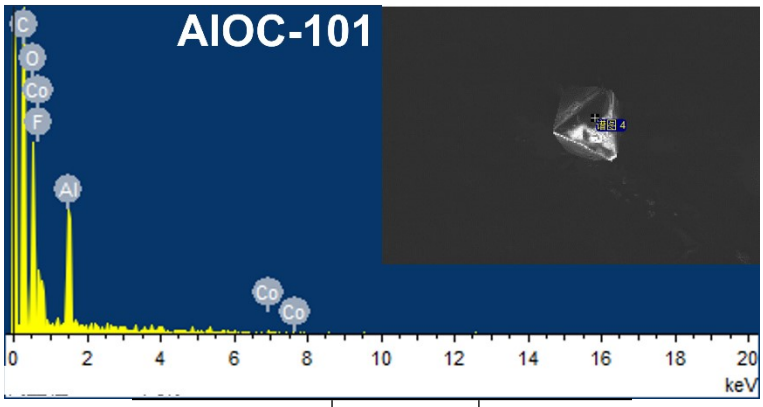

Elements	Wt. %	Mol.%
C	48.66	62.42
O	25.79	24.83
F	8.62	6.99
Co	12.62	3.30
Al	4.31	2.46

Fig. S49. The EDS spectrum and quantitative analysis of **AlOC-101**.

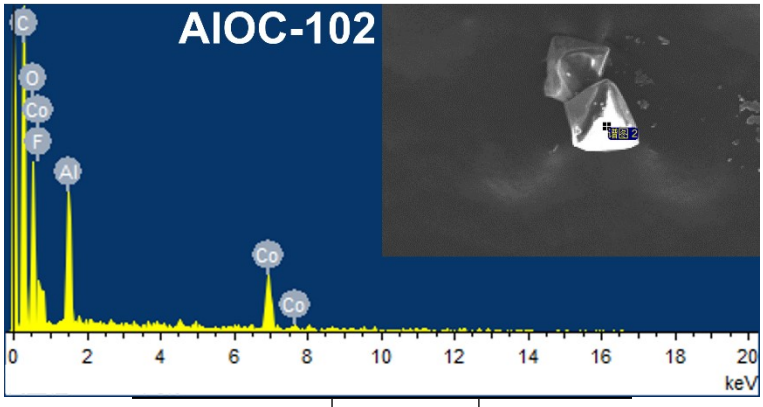

Elements	Wt. %	Mol.%
C	54.81	67.65
O	21.30	19.74
F	9.54	7.44
Co	9.13	2.30

Al	5.22	2.87

Fig. S50. The EDS spectrum and quantitative analysis of **AlOC-102**.

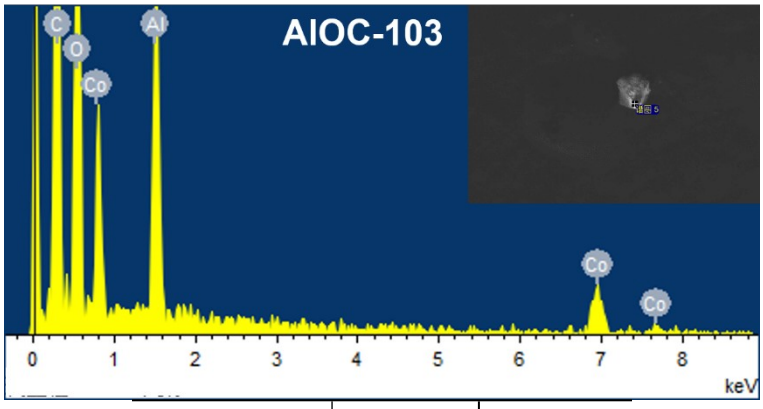

Elements	Wt. %	Mol.%
C	48.07	61.11
O	34.50	32.93
Co	12.71	3.29
Al	4.72	2.67

Fig. S51. The EDS spectrum and quantitative analysis of **AlOC-103**.

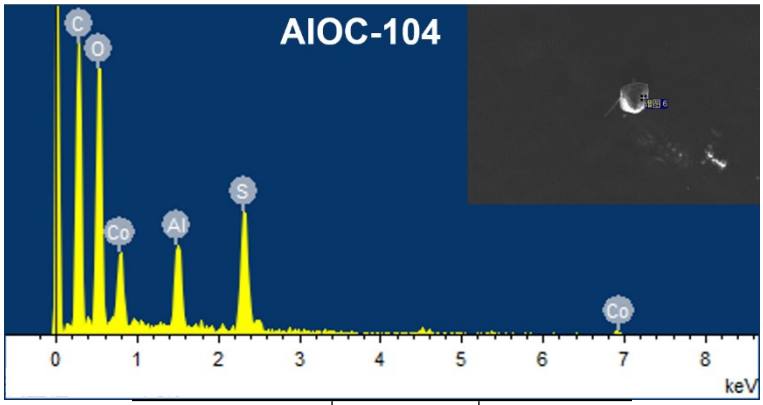

Elements	Wt. %	Mol.%
C	37.08	53.60
O	27.07	29.38
S	18.66	10.11
Co	11.87	3.50
Al	5.32	3.41

Fig. S52. The EDS spectrum and quantitative analysis of **AlOC-104**.

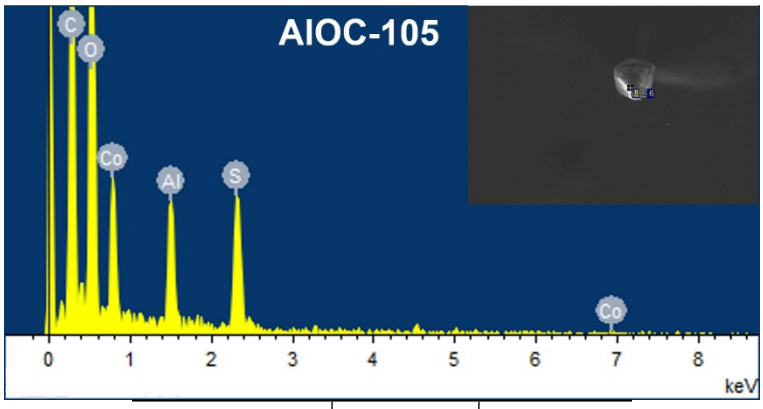

Elements	Wt. %	Mol.%
C	42.14	58.89
O	23.43	24.58
S	19.55	10.24
Co	8.78	2.50
Al	6.10	3.79

Fig. S53. The EDS spectrum and quantitative analysis of **AlOC-105**.

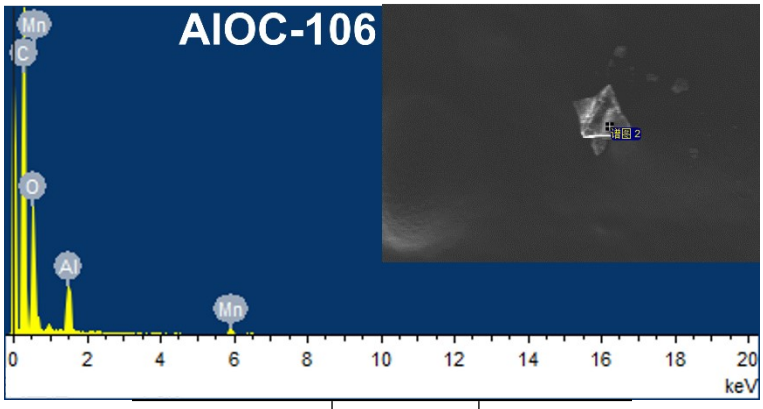

Elements	Wt. %	Mol.%
C	50.74	63.06
O	33.65	31.40
Mn	10.98	2.98
Al	4.63	2.56

Fig. S54. The EDS spectrum and quantitative analysis of **AlOC-106**.

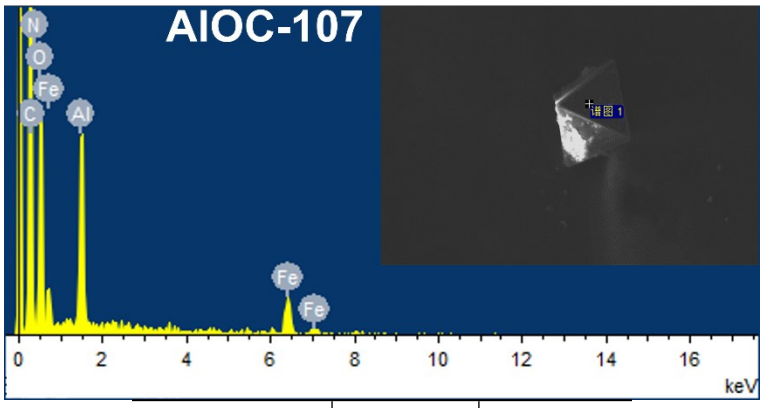

Elements	Wt. %	Mol.%
C	56.14	66.43
O	33.72	29.86
N	0.41	0.27
Fe	3.58	1.88
Al	6.15	1.56

Fig. S55. The EDS spectrum and quantitative analysis of **AlOC-107**.

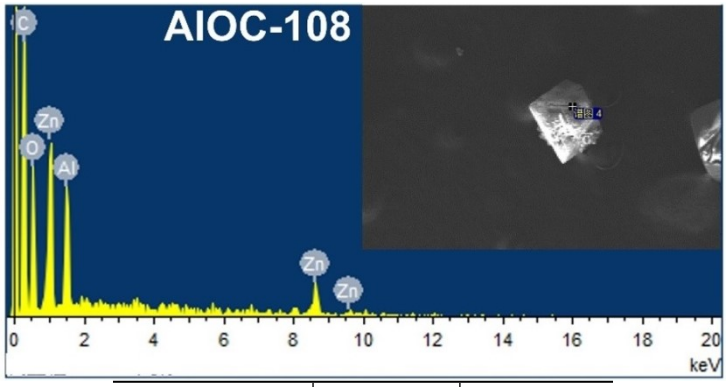

Elements	Wt. %	Mol.%
C	59.70	74.65
O	19.69	18.48
Zn	14.10	3.24
Al	6.51	3.63

Fig. S56. The EDS spectrum and quantitative analysis of **AlOC-108**.

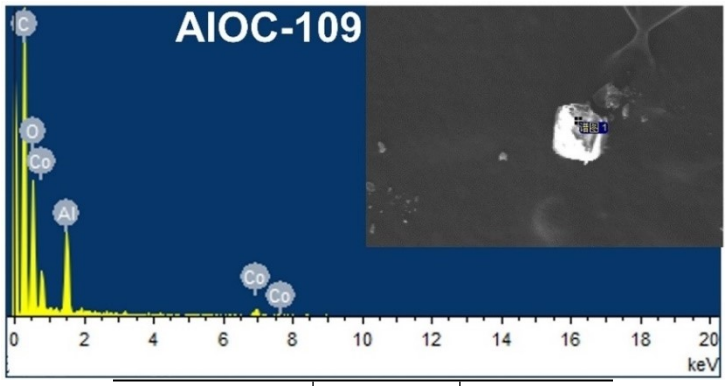

Elements	Wt. %	Mol.%
C	62.27	74.98
O	22.07	19.95
Co	11.43	2.81
Al	4.23	2.26

Fig. S57. The EDS spectrum and quantitative analysis of **AlOC-109**.

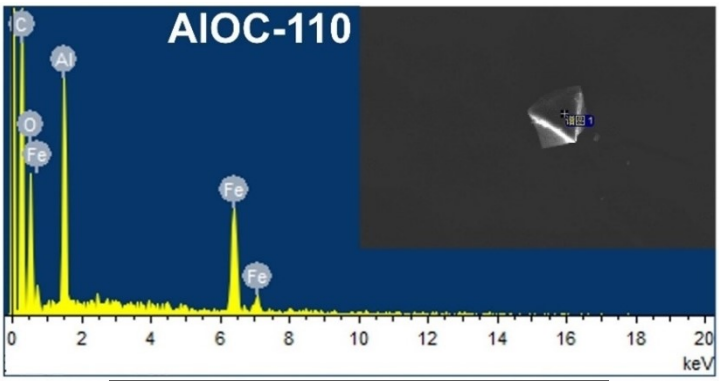

Elements	Wt. %	Mol.%
C	52.76	66.29
O	28.59	26.97
Fe	12.76	3.45
Al	5.89	3.29

Fig. S58. The EDS spectrum and quantitative analysis of **AlOC-110**.

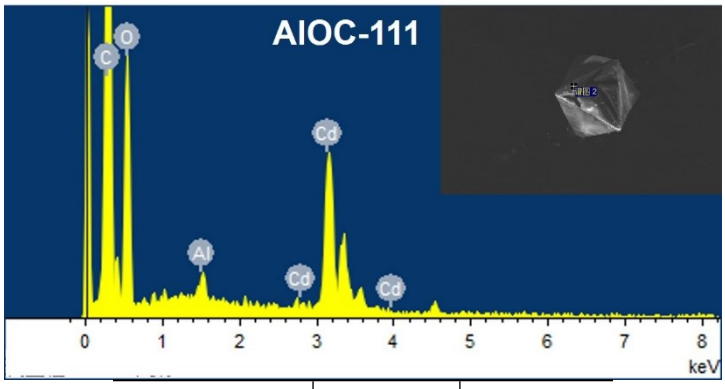

Elements	Wt. %	Mol.%
C	55.31	73.30
O	21.02	20.91
Cd	18.24	2.58
Al	5.43	3.21

Fig. S59. The EDS spectrum and quantitative analysis of **AlOC-111**.

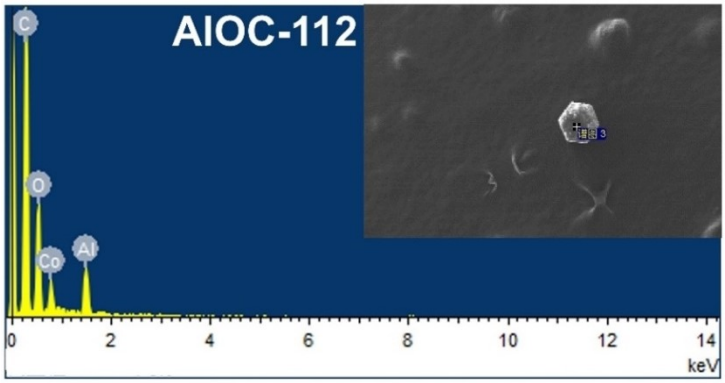

Elements	Wt. %	Mol.%
C	58.34	70.50
O	26.49	24.03
Co	9.21	2.27
Al	5.96	3.20

Fig. S60. The EDS spectrum and quantitative analysis of **AlOC-112**.

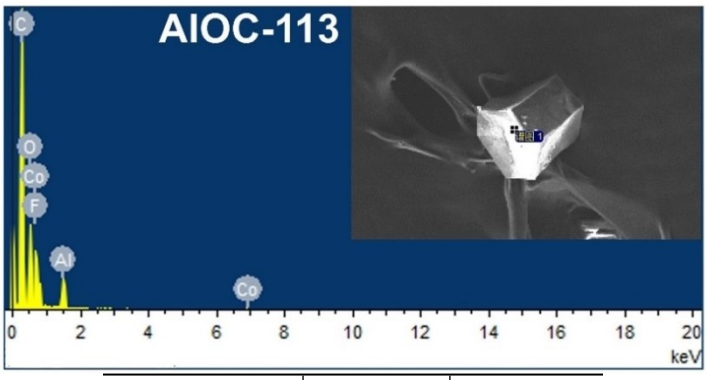

Elements	Wt. %	Mol.%
C	54.67	69.02
O	15.92	15.09
F	12.37	9.87
Co	11.66	3.00
Al	5.38	3.02

Fig. S61. The EDS spectrum and quantitative analysis of **AlOC-113**.

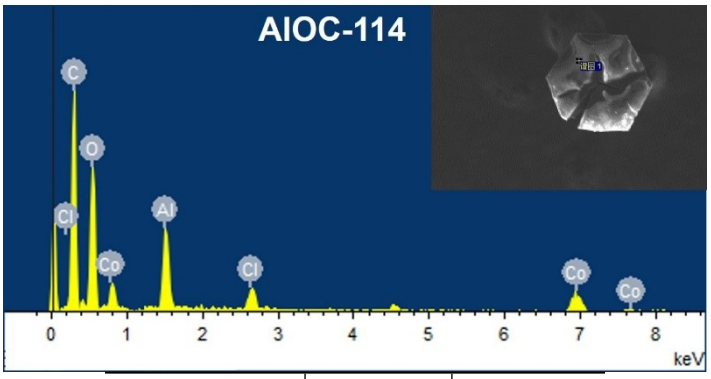

Elements	Wt. %	Mol.%
C	49.42	68.41
O	15.84	16.46
Cl	19.66	9.22
Co	10.12	2.86
Al	4.96	3.05

Fig. S62. The EDS spectrum and quantitative analysis of **AlOC-114**.

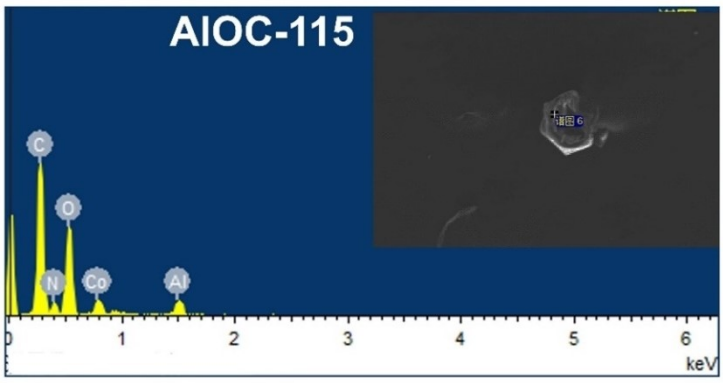

Elements	Wt. %	Mol.%
C	59.65	72.18
O	23.75	21.57
N	1.22	1.27
Co	11.30	2.79
Al	4.08	2.19

Fig. S63. The EDS spectrum and quantitative analysis of **AlOC-115**.

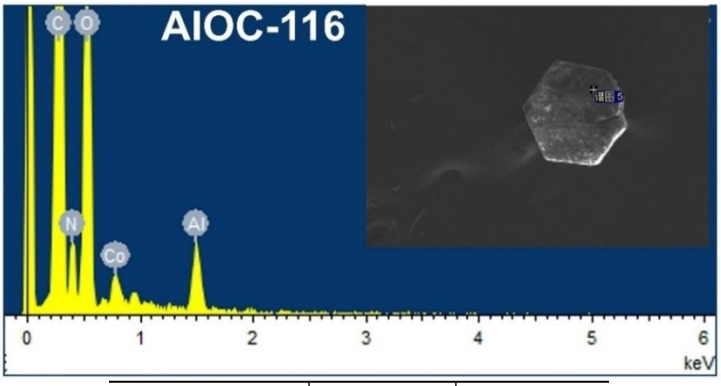

Elements	Wt. %	Mol.%
C	54.29	66.80
O	21.33	19.70
N	7.68	8.10
Co	12.66	3.18
Al	4.04	2.22

Fig. S64. The EDS spectrum and quantitative analysis of **AlOC-116**.

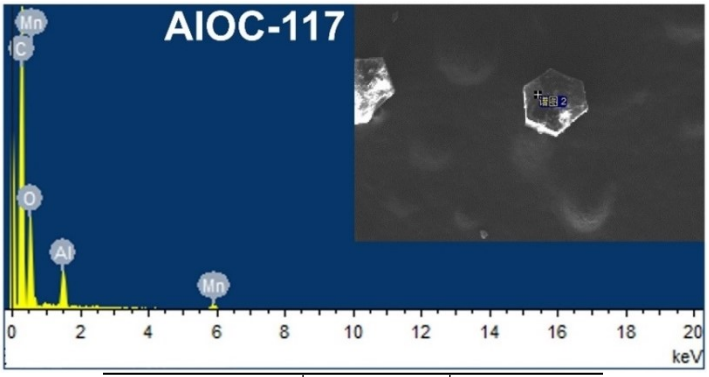

Elements	Wt. %	Mol.%
C	59.24	73.30
O	20.96	19.47
Mn	13.11	3.55
Al	6.69	3.68

Fig. S65. The EDS spectrum and quantitative analysis of **AlOC-117**.

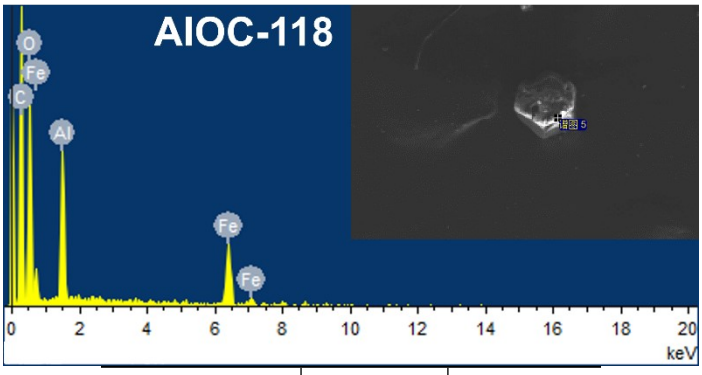

Elements	Wt. %	Mol.%
C	60.86	70.85
O	29.61	25.88
Fe	6.21	1.55
Al	3.32	1.72

Fig. S66. The EDS spectrum and quantitative analysis of **AlOC-118**.

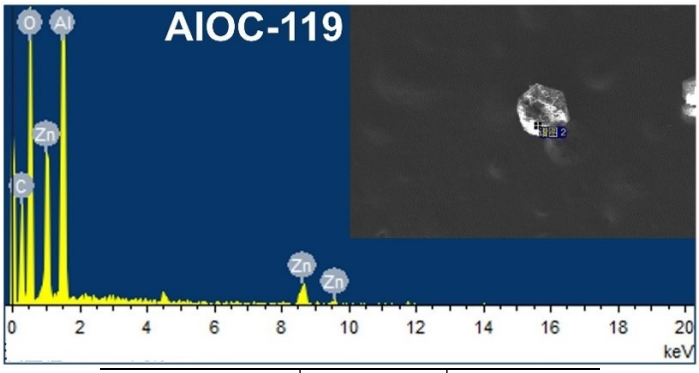

Elements	Wt. %	Mol.%
C	59.42	74.55
O	19.69	18.55
Zn	14.52	3.35
Al	6.37	3.55

Fig. S67. The EDS spectrum and quantitative analysis of **AlOC-119**.

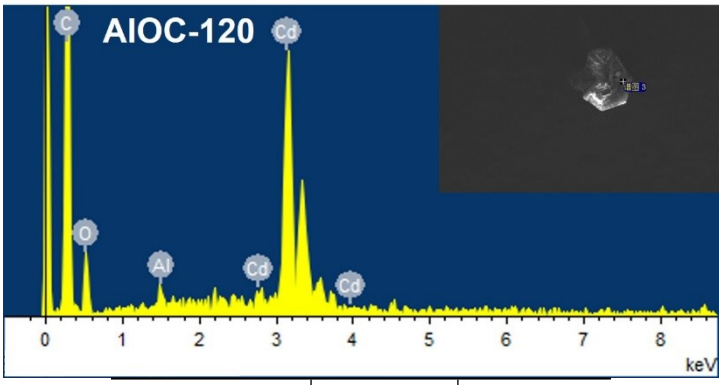

Elements	Wt. %	Mol.%
C	57.39	77.59
O	15.40	15.63
Cd	20.97	3.03
Al	6.24	3.75

Fig. S68. The EDS spectrum and quantitative analysis of **AlOC-120**.

Discussion for EDS spectra:

The EDS spectra of **AlOC-99** to **AlOC-120** were used to confirm the existence of metal elements. Also, the quantification of metal elements was determined (Fig. S47–S68). The molar ratios between Al and M are approximately 1, which are consistent with the formula.

12. The XPS spectra.

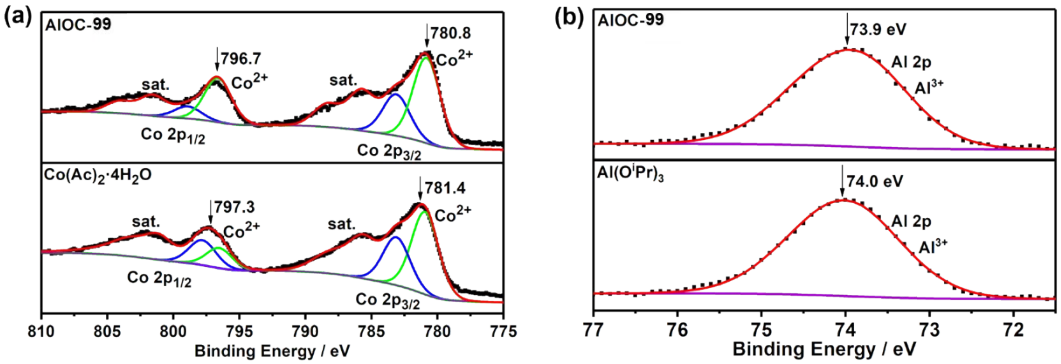

Fig. S69. The Co 2p and Al 2p XPS spectra of **AlOC-99**, $Co(Ac)_2{\cdot}4H_2O$ and $Al(O^iPr)_3$.

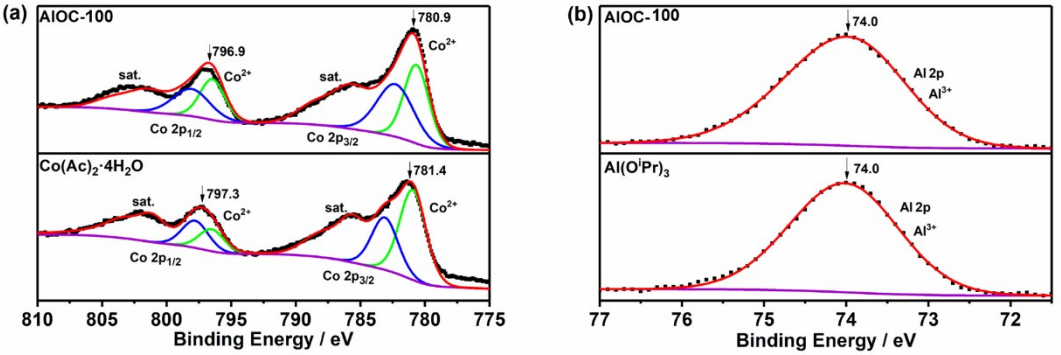

Fig. S70. The Co 2p and Al 2p XPS spectra of **AlOC-100**, $Co(Ac)_2{\cdot}4H_2O$ and $Al(O^iPr)_3$.

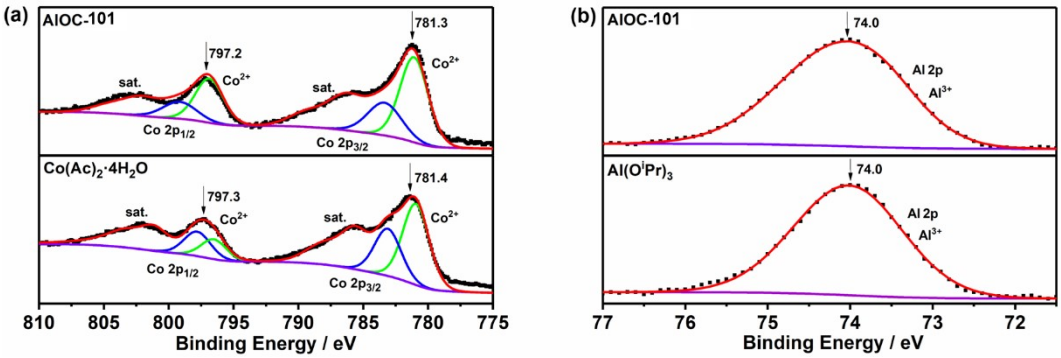

Fig. S71. The Co 2p and Al 2p XPS spectra of **AlOC-101**, $Co(Ac)_2{\cdot}4H_2O$ and $Al(O^iPr)_3$.

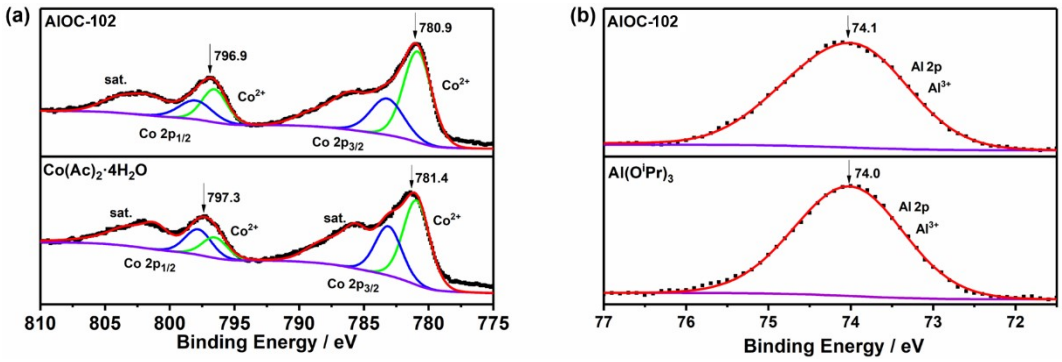

Fig. S72. The Co 2p and Al 2p XPS spectra of **AlOC-102**, $Co(Ac)_2{\cdot}4H_2O$ and $Al(O^iPr)_3$.

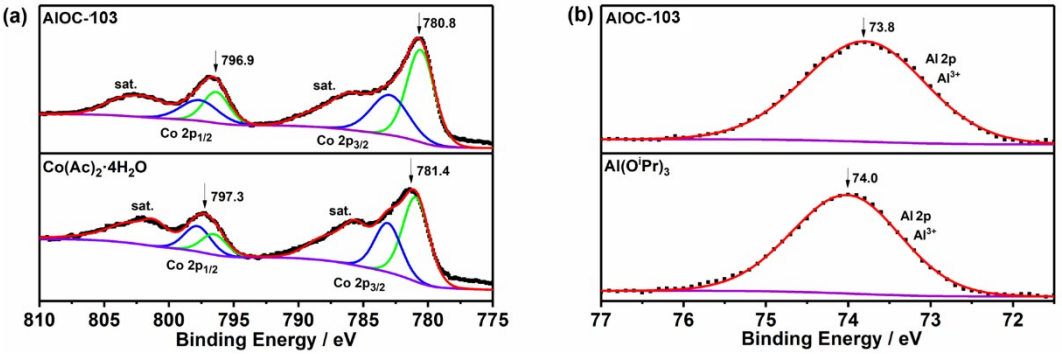

Fig. S73. The Co 2p and Al 2p XPS spectra of **AlOC-103**, $Co(Ac)_2{\cdot}4H_2O$ and $Al(O^iPr)_3$.

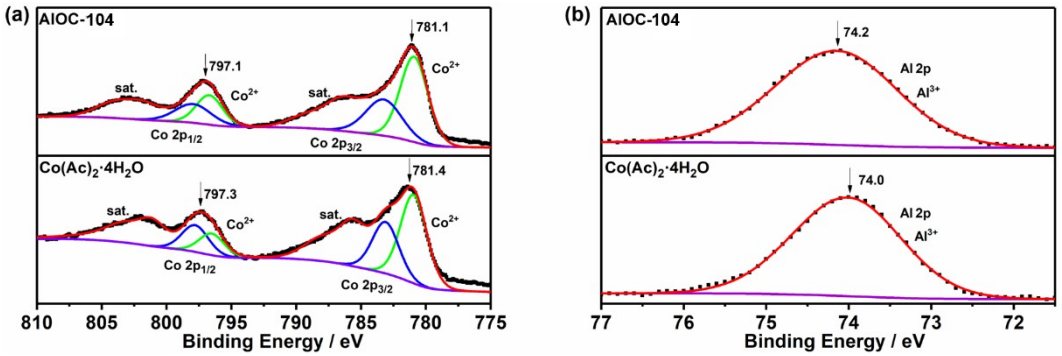

Fig. S74. The Co 2p and Al 2p XPS spectra of **AlOC-104**, $Co(Ac)_2{\cdot}4H_2O$ and $Al(O^iPr)_3$.

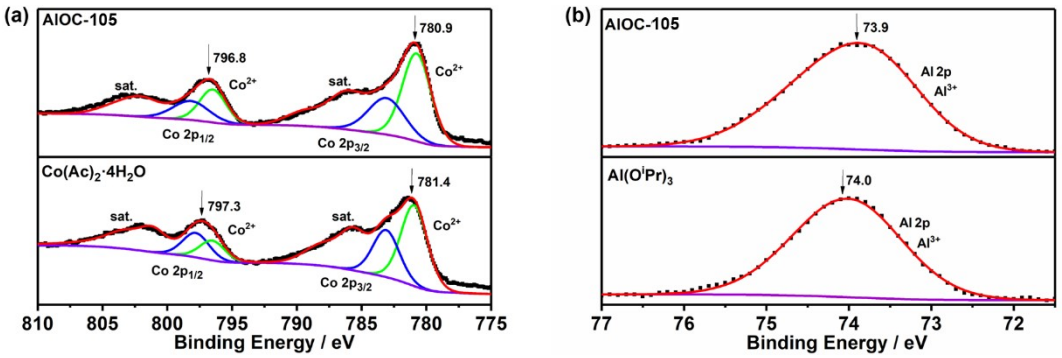

Fig. S75. The Co 2p and Al 2p XPS spectra of **AlOC-105**, $Co(Ac)_2{\cdot}4H_2O$ and $Al(O^iPr)_3$.

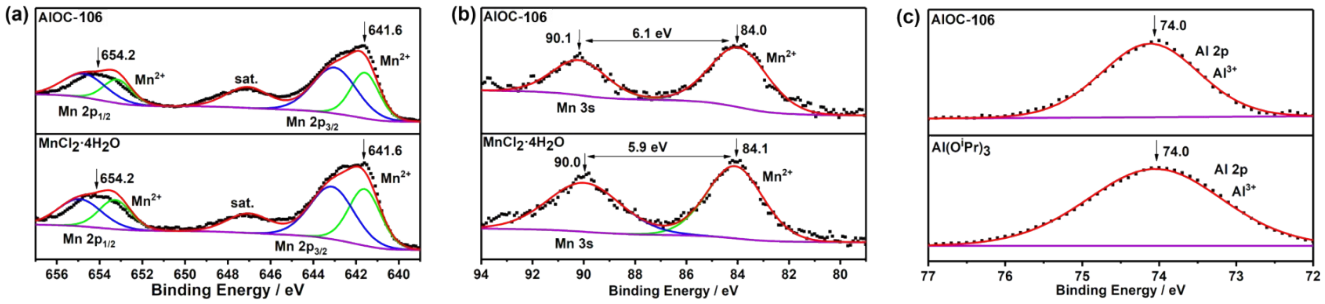

Fig. S76. The Mn 2p, Mn 3s and Al 2p XPS spectra of **AlOC-106**, $MnCl_2{\cdot}4H_2O$ and $Al(O^iPr)_3$.

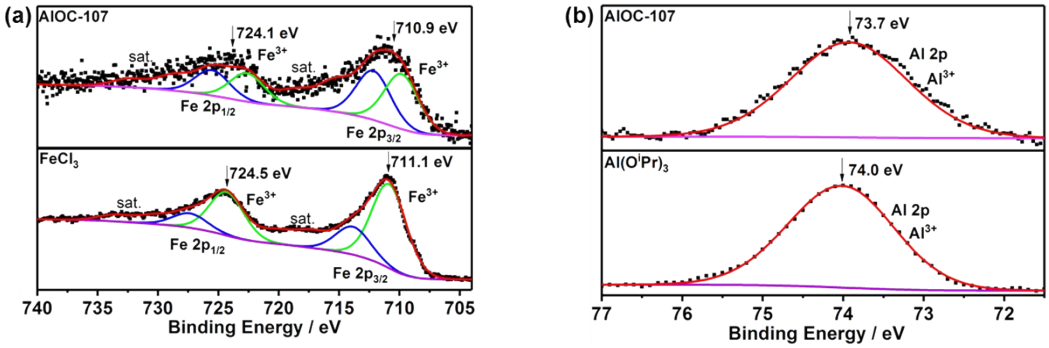

Fig. S77. The Fe 2p and Al 2p XPS spectra of **AlOC-107**, $FeCl_3$ and $Al(O^iPr)_3$.

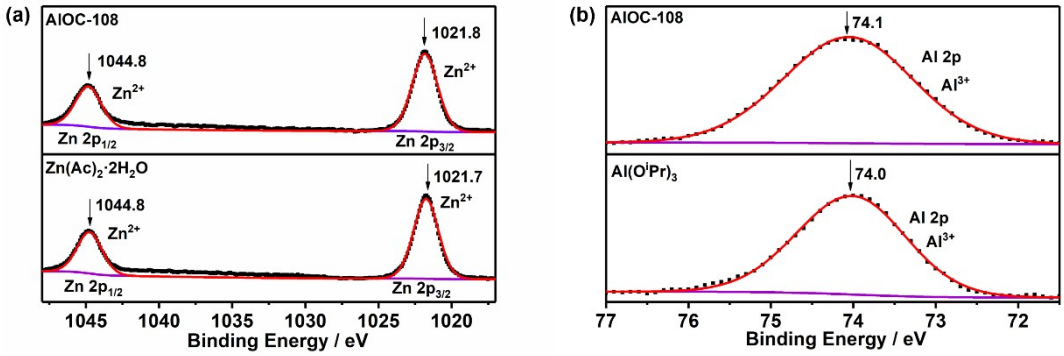

Fig. S78. The Zn 2p and Al 2p XPS spectra of **AlOC-108**, $Zn(Ac)_2{\cdot}2H_2O$ and $Al(O^iPr)_3$.

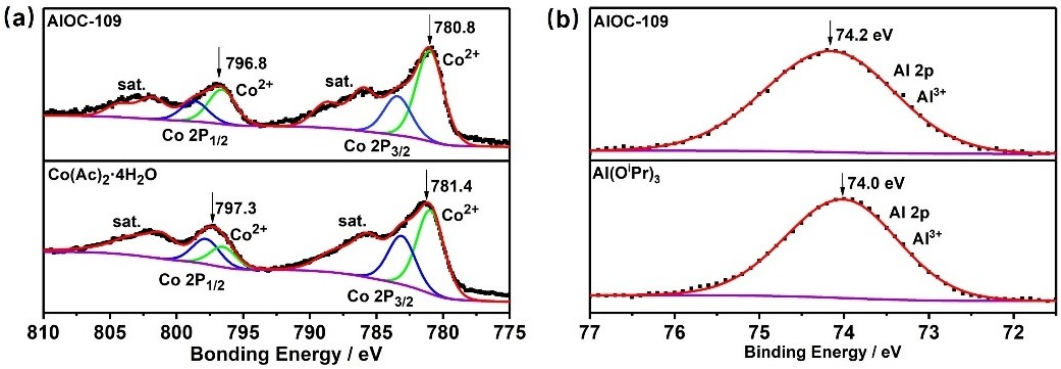

Fig. S79. The Co 2p and Al 2p XPS spectra of **AlOC-109**, $Co(Ac)_2{\cdot}4H_2O$ and $Al(O^iPr)_3$.

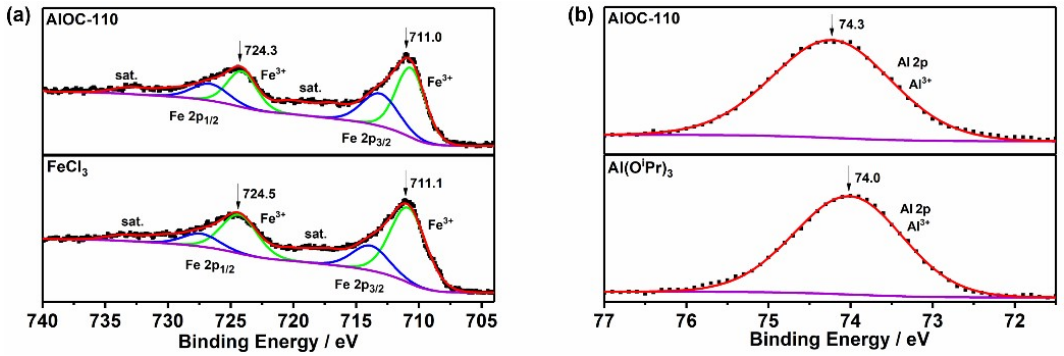

Fig. S80. The Fe 2p and Al 2p XPS spectra of **AlOC-110**, $FeCl_3$ and $Al(O^iPr)_3$.

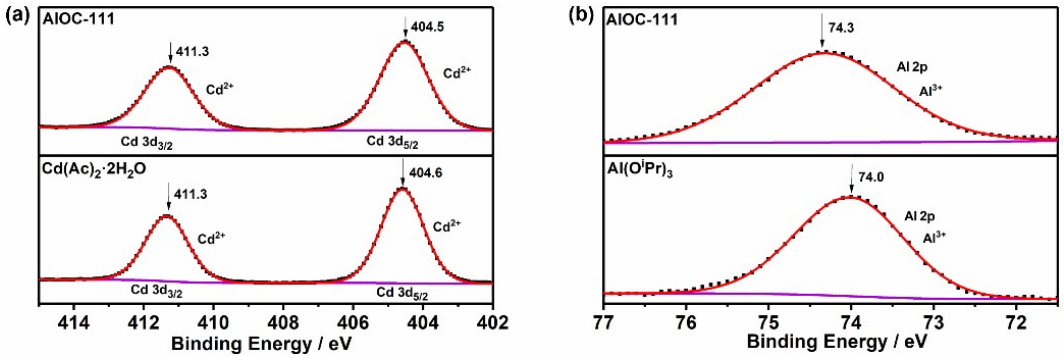

Fig. S81. The Cd 3d and Al 2p XPS spectra of **AlOC-111**, $Cd(Ac)_2{\cdot}2H_2O$ and $Al(O^iPr)_3$.

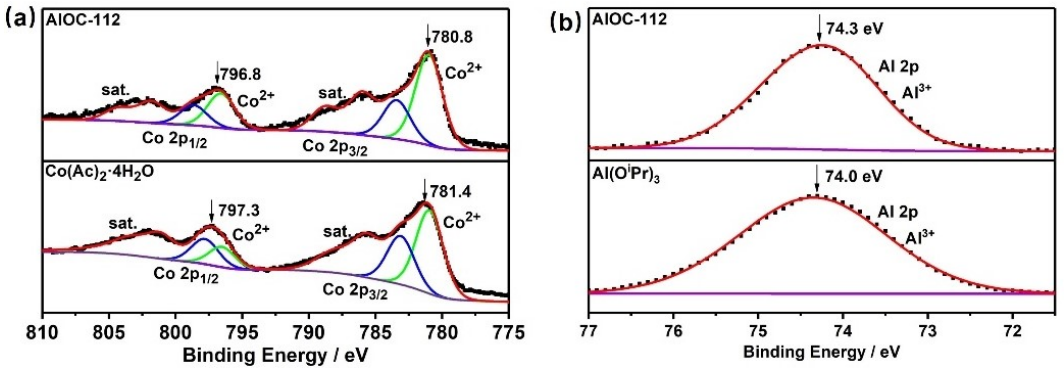

Fig. S82. The Co 2p and Al 2p XPS spectra of **AlOC-112**, $Co(Ac)_2{\cdot}4H_2O$ and $Al(O^iPr)_3$.

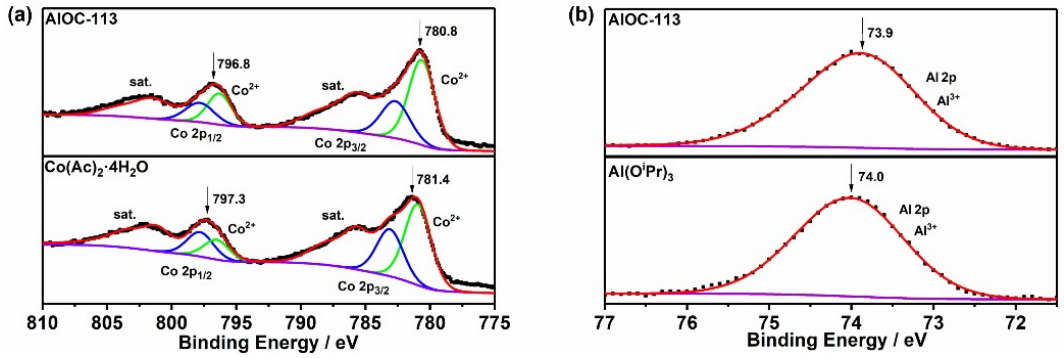

Fig. S83. The Co 2p and Al 2p XPS spectra of **AlOC-113**, $Co(Ac)_2{\cdot}4H_2O$ and $Al(O^iPr)_3$.

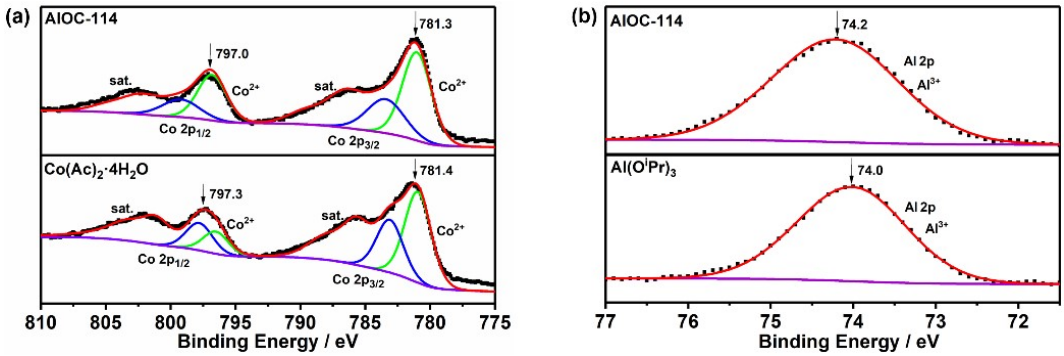

Fig. S84. The Co 2p and Al 2p XPS spectra of **AlOC-114**, $Co(Ac)_2{\cdot}4H_2O$ and $Al(O^iPr)_3$.

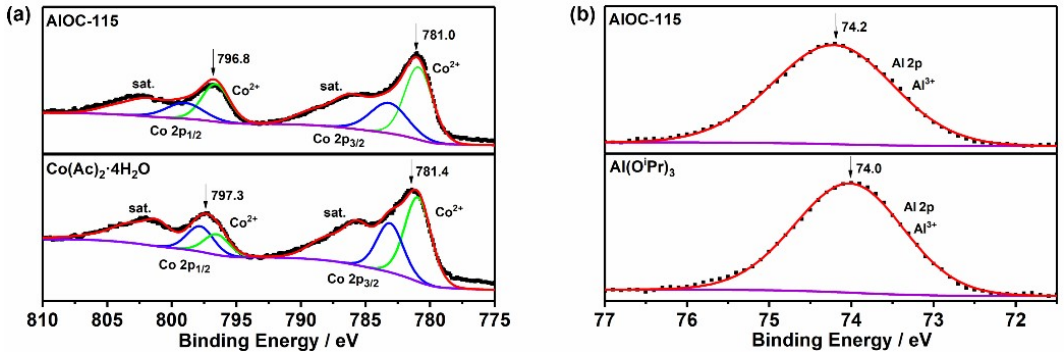

Fig. S85. The Co 2p and Al 2p XPS spectra of **AlOC-115**, $Co(Ac)_2{\cdot}4H_2O$ and $Al(O^iPr)_3$.

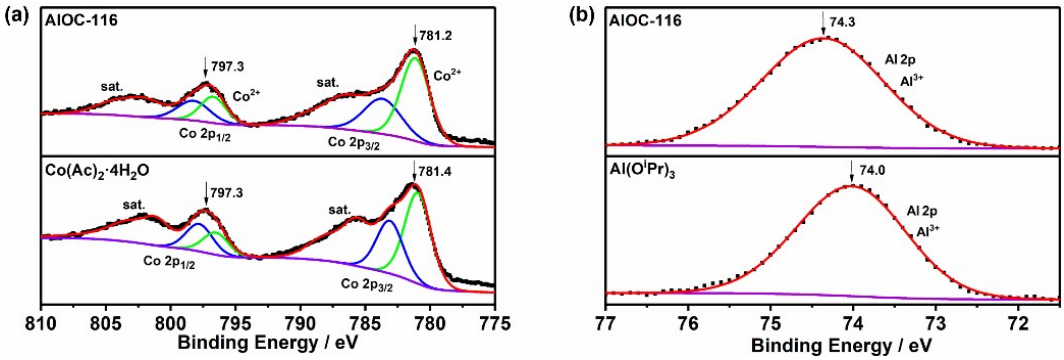

Fig. S86. The Co 2p and Al 2p XPS spectra of **AlOC-116**, $Co(Ac)_2{\cdot}4H_2O$ and $Al(O^iPr)_3$.

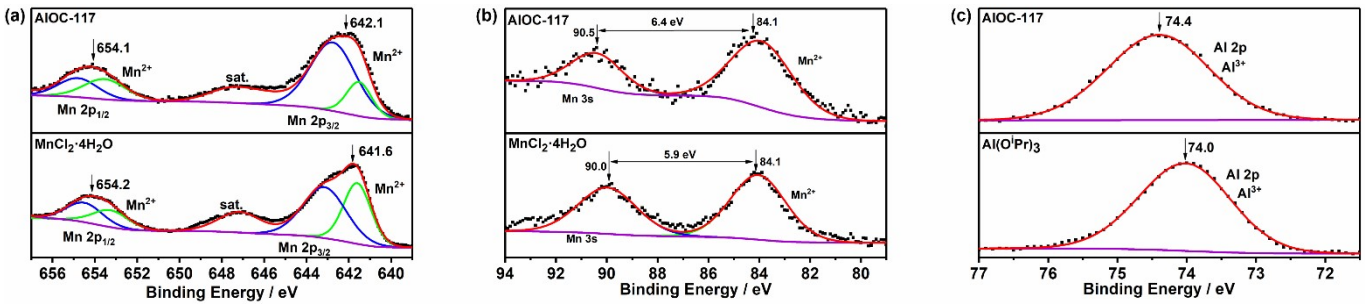

Fig. S87. The Mn 2p, Mn 3s and Al 2p XPS spectra of **AlOC-117**, $MnCl_2{\cdot}4H_2O$ and $Al(O^iPr)_3$.

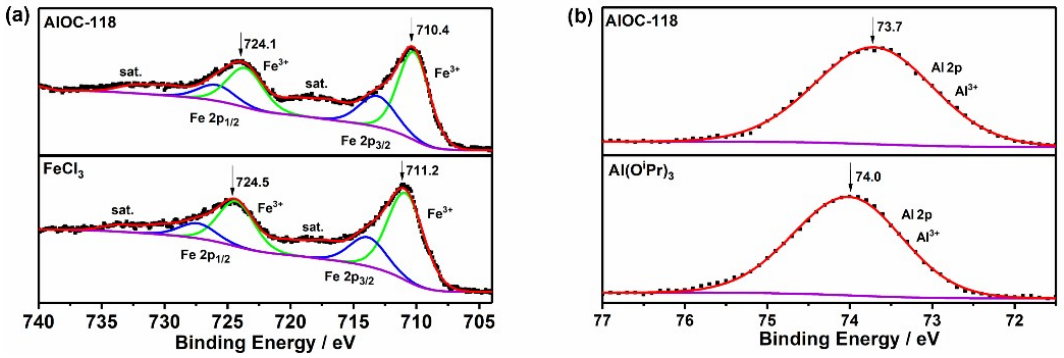

Fig. S88. The Fe 2p and Al 2p XPS spectra of **AlOC-118**, $FeCl_3$ and $Al(O^iPr)_3$.

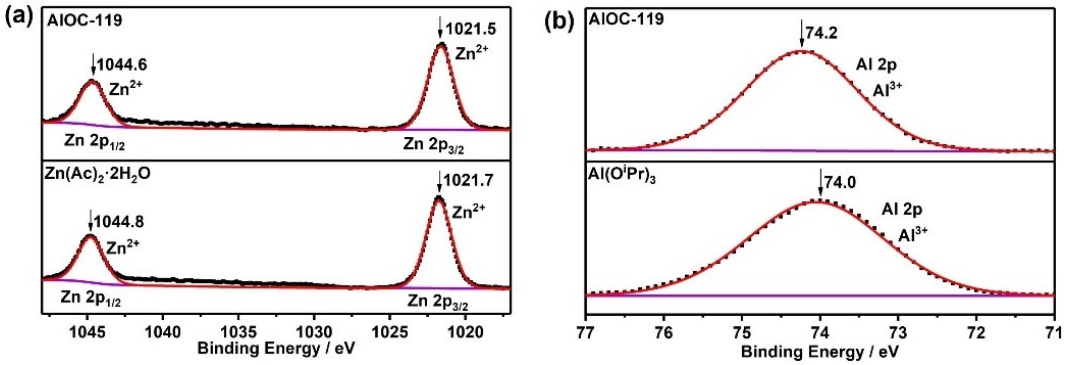

Fig. S89. The Zn 2p and Al 2p XPS spectra of **AlOC-119**, $Zn(Ac)_2{\cdot}2H_2O$ and $Al(O^iPr)_3$.

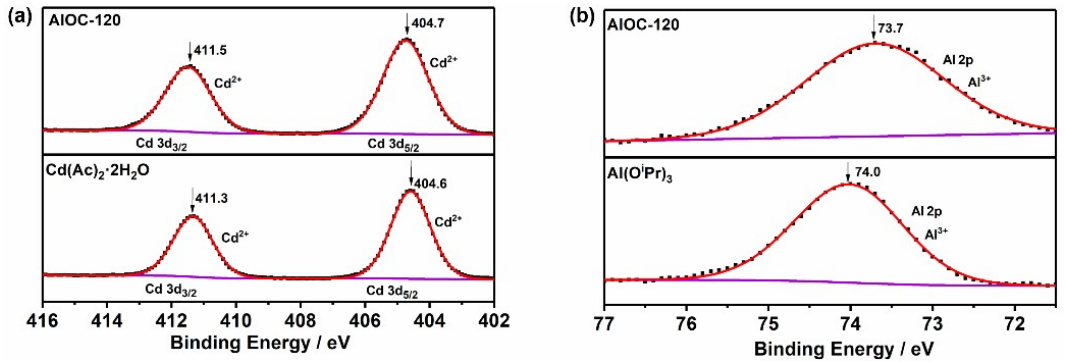

Fig. S90. The Cd 3d and Al 2p XPS spectra of **AlOC-120**, $Cd(Ac)_2{\cdot}2H_2O$ and $Al(O^iPr)_3$.

Discussion for XPS spectra:

The XPS measurements of **AlOC-99** to **AlOC-120** were conducted to verify the valence states of metal ions in frameworks. The high-resolution Co 2p spectra exhibit two main regions of Co $2p_{1/2}$ and Co $2p_{3/2}$ with ca. 16 eV binding energy difference (Fig. S69–S75, S79, and S82–S86).[1-2] In Co $2p_{1/2}$ region, it can be deconvoluted into two peaks of Co^{2+} at 796.7–797.3 eV and the corresponding shake-up satallite peak at 801.8–802.7 eV. Similarly, Co $2p_{3/2}$ region also demonstrates two peaks of Co^{2+} (780.8–781.4 eV) and a relevant satellite peak (785.8–786.4 eV). The two satellite peaks are assigned to the shakeup excitation of high-spin Co^{2+} ions. The Mn 2p spectra of **AlOC-106** and **AlOC-117** are split into two components at 641.6–642.1 eV (Mn $2p_{3/2}$) and 654.1–654.2 eV (Mn $2p_{1/2}$), with a satellite peak located at 647.1–647.3 eV (Fig. S76 and S87).[3] These binding energies are consistent with an Mn^{2+} cation as reported for manganese oxide.[4] The Mn 3s core peak allows us to confirm the oxidation of Mn.[5] The splitting of this peak is dependent on the number of 3d electrons, and expected values are ~6.5 eV for Mn^{2+}, ~5.5 eV for Mn^{3+}, and ~4.5 eV for Mn^{4+}. Here, the splitting value for **AlOC-106** and **AlOC-117** are respectively ~6.1 eV and 6.4 eV (Fig. S76b and S87b), indicated the existence of Mn^{2+} in crystals. For **AlOC-108** and **AlOC-119**, the observed Zn $2p_{1/2}$ and Zn $2p_{3/2}$ are located at 1044.6–1044.8 eV and 1021.5–1021.8 eV, corresponding to Zn^{2+} species (Fig. S78 and S89).[6-7] In Fig. S81 and S90, two peaks locate at about 411.3–411.5 eV and 404.5–404.7 eV, matched well with the spin-orbit seperation between Cd $3d_{5/2}$ and Cd $3d_{3/2}$ of Cd^{2+} in frameworks.[8] The Fe XPS analysis for **AlOC-107**, **AlOC-110** and **AlOC-118** were also researched, however, the obvious Fe^{3+} signals were captured (Fig. S77, S80 and S88), which is inconsistency with BVS results.[9] This maybe owing to the rapid oxidation of external Fe^{2+} specieses when freshly prepared crystals were exposed into air. The Al 2p signals only contain one peak centered at 73.9–74.3 eV, consistent with the literature value for Al^{3+}.[10] Besides, the characteristic XPS peaks of **AlOC-99** to **AlOC-120** are in agreement with pure metal salts and $Al(O^iPr)_3$.

13. The UV-vis absorption spectra and Tau plots.

Fig. S91. The crystal colour of **AIOC-110** before and after exposing in air.

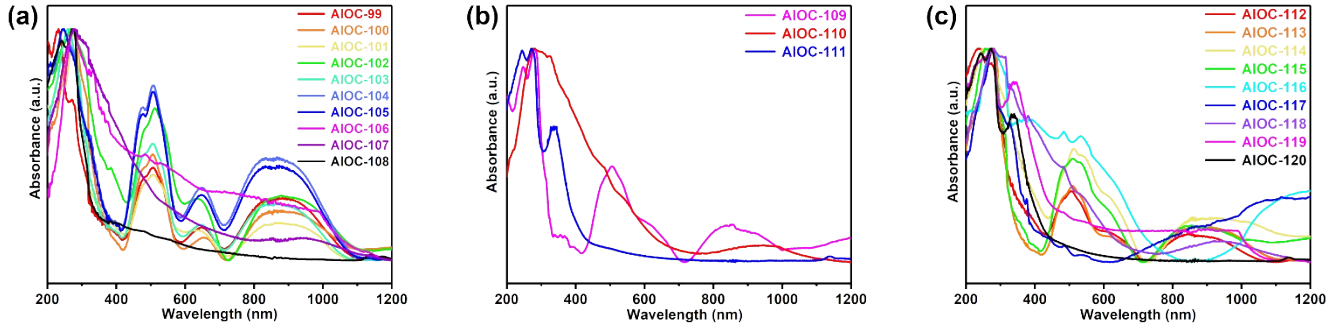

Fig. S92. The UV-vis absorption spectra.

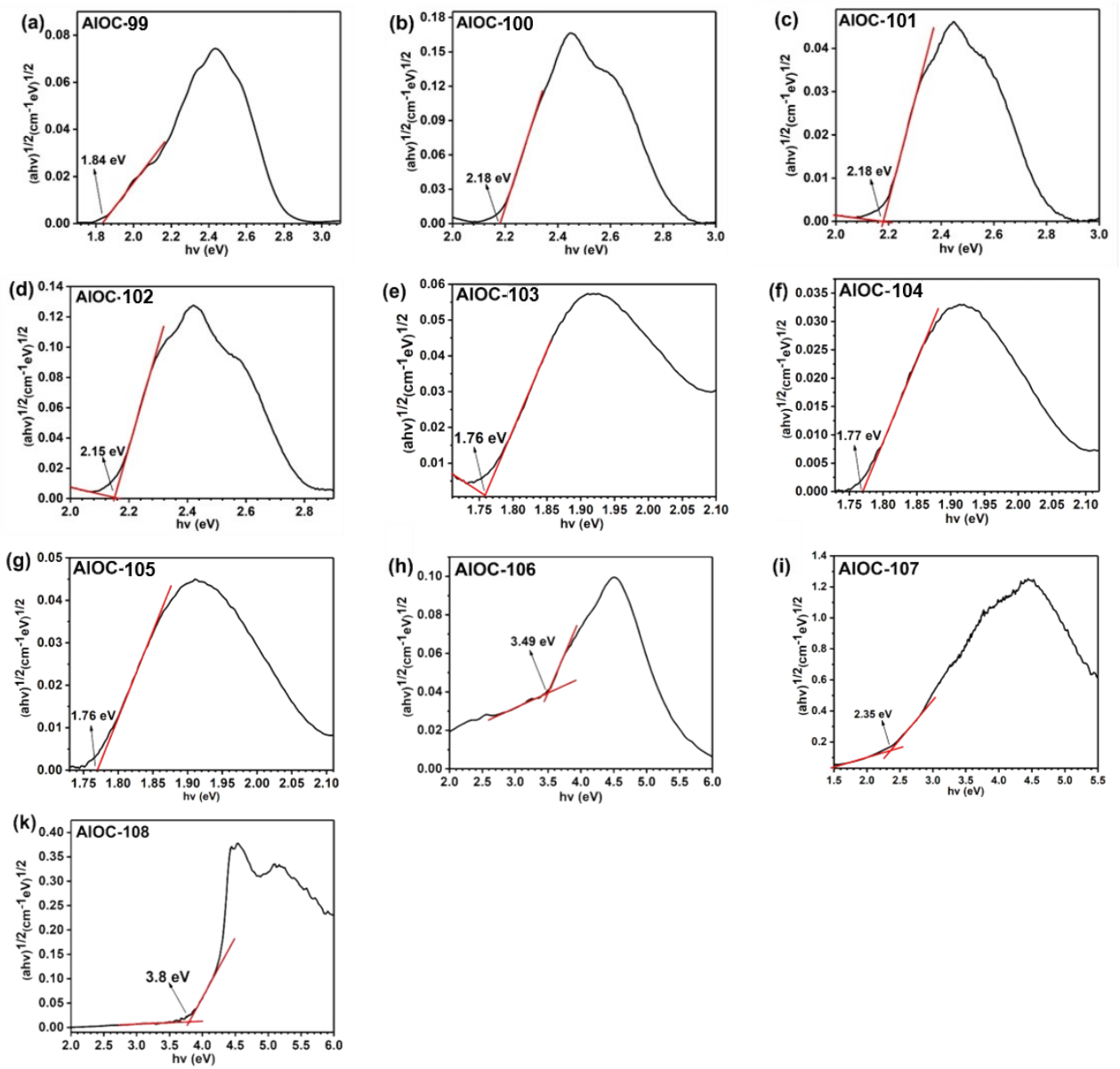

Fig. S93. Tau plots of two-fold interpenetrated diamond (***dia***) frameworks based on UV-vis diffuse reflectance spectra.

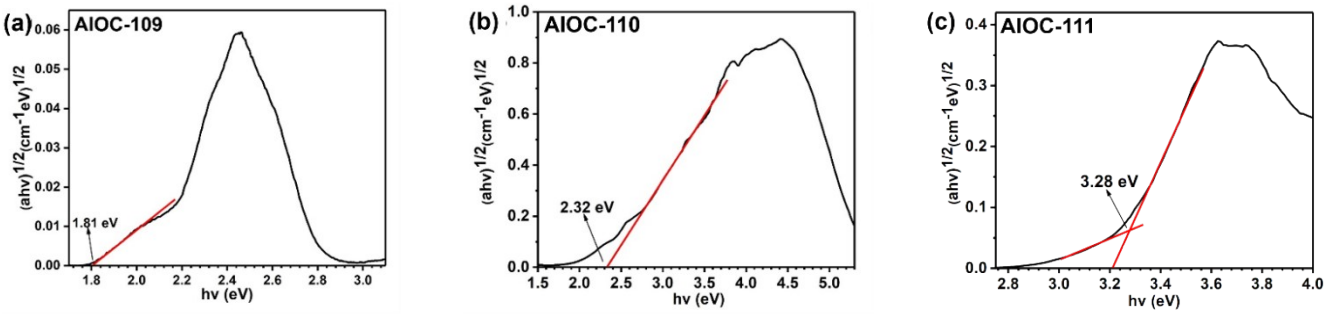

Fig. S94. Tau plots of non-interpenetrated diamond (***dia***) frameworks based on UV-vis diffuse reflectance spectra.

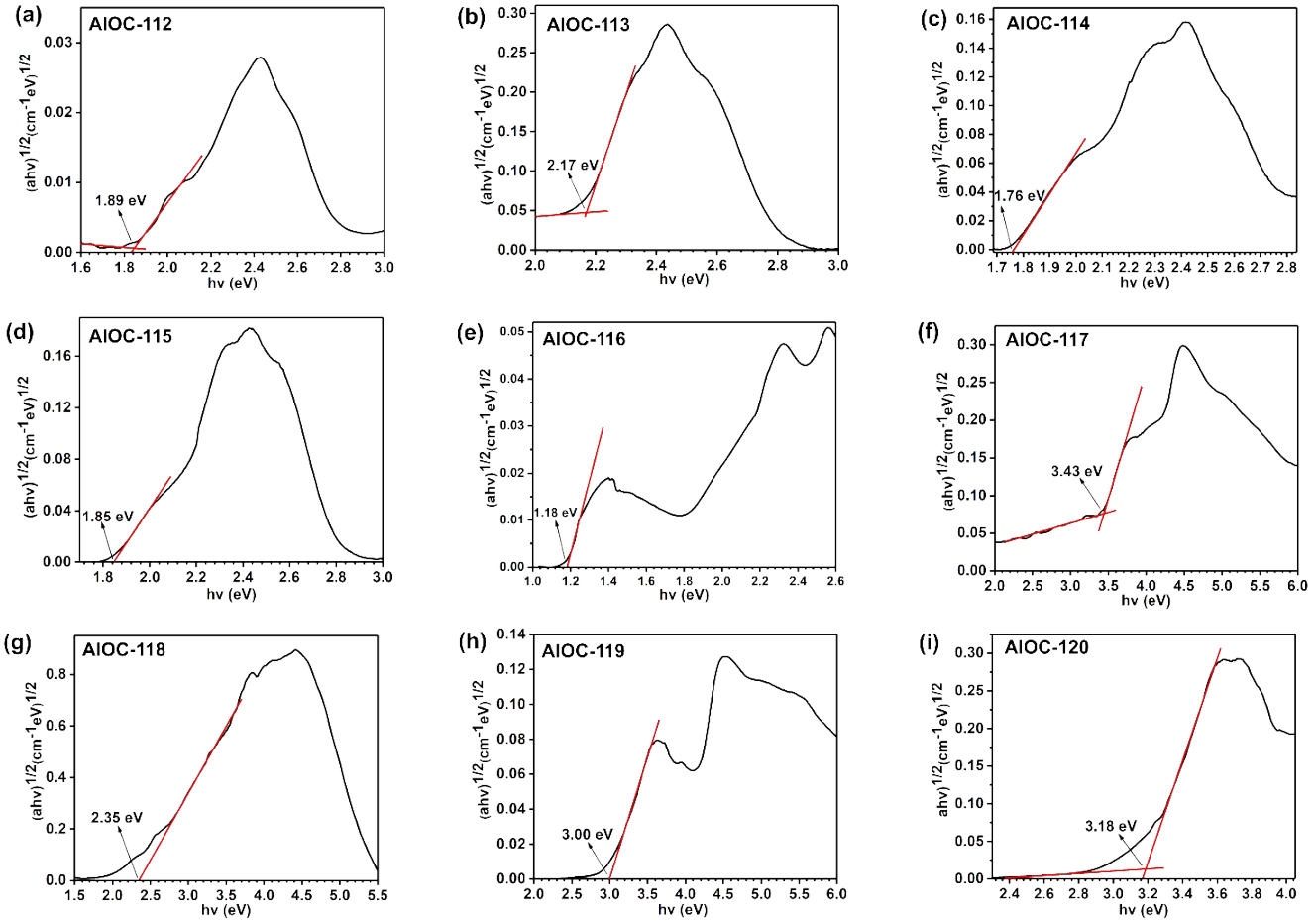

Fig. S95. Tau plots of non-interpenetrated lonsdaleite (***lon***) frameworks based on UV-vis diffuse reflectance spectra.

14. Catalytic stability.

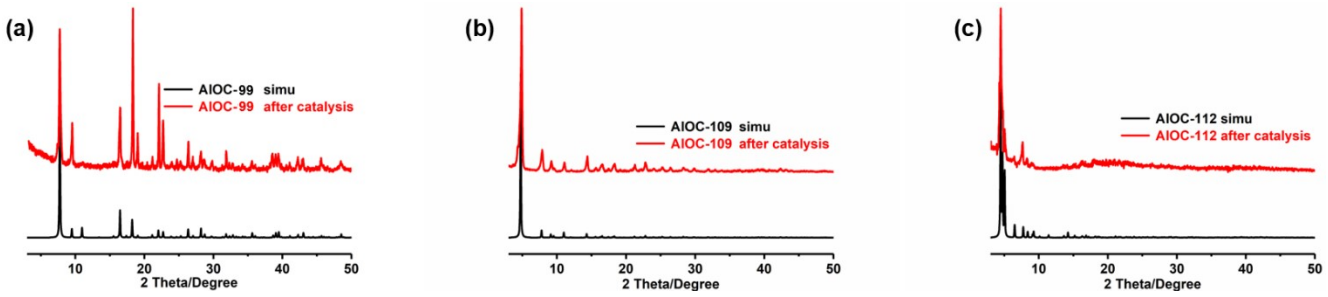

Fig. S96. PXRD patterns of **AlOC-99**, **AlOC-109** and **AlOC-112** after catalysis.

Tables

Table S1. Crystallographic data and structure refinement parameters for two-fold interpenetrated diamond (***dia***) frameworks (**AlOC-99** to **AlOC-103**).

	AlOC-99	**AlOC-100**	**AlOC-101**	**AlOC-102**	**AlOC-103**
Empirical formula	$C_{96}H_{84}Al_4Co_4N_4O_{28}$	$C_{96}H_{72}Al_4Co_4F_{12}N_4O_{28}$	$C_{96}H_{72}Al_4Co_4F_{12}N_4O_{28}$	$C_{96}H_{72}Al_4Co_4F_{12}N_4O_{28}$	$C_{72}H_{60}Al_4Co_4N_4O_{40}$
Formula weight	2085.39	2301.30	2301.21	2301.21	1964.96
Temperature / K	105.61(11) K	106.15(10) K	105.66(11) K	105.94(10) K	105.63(19) K
Crystal system	Cubic	Cubic	Cubic	Cubic	Cubic
Space group	*F*d-3*c*	*F*d-3*c*	*F*d-3*c*	*F*d-3*c*	*F*d-3*c*
a [Å]	32.2520(2)	32.1911(2)	32.3063(3)	32.7575(6)	31.6599(6)
b [Å]	32.2520(2)	32.1911(2)	32.3063(3)	32.7575(6)	31.6599(6)
c [Å]	32.2520(2)	32.1911(2)	32.3063(3)	32.7575(6)	31.6599(6)
α [°]	90	90	90	90	90
B [°]	90	90	90	90	90
γ [°]	90	90	90	90	90
V [Å^3]	33548.3(6)	33358.6(6)	33718.0(9)	35150.6(19)	31734.3(18)
Z	15.99936	15.99936	16	16	15.99936
ρ_{calcd} [g cm^{-3}]	1.651	1.833	1.813	1.739	1.645
μ [mm^{-1}]	4.958	5.168	5.114	4.905	5.288
F (000)	17152.0	18688.0	18688.0	18688.0	16000.0
Index ranges	−26 ≤ h ≤ 38 −41 ≤ k ≤ 39 −19 ≤ l ≤ 29	−38 ≤ h ≤ 40 −26 ≤ k ≤ 33 −28 ≤ l ≤ 40	−39 ≤ h ≤ 24 −40 ≤ k ≤ 25 −24 ≤ l ≤ 31	−22 ≤ h ≤ 39 −21 ≤ k ≤ 36 −31 ≤ l ≤ 40	−17 ≤ h ≤ 30 −39 ≤ k ≤ 21 −19 ≤ l ≤ 29
Reflns collected	10409	9217	9405	9910	9217
unique reflns [R_{int}]	1586[0.0212]	1435 [0.0223]	1405 [0.0384]	1503 [0.1526]	1350[0.0507]
data/restraints/parameters	1586/84/128	1435/78/160	1405/57/109	1503/37/101	1350/0/94
GOF on F^2	1.056	1.126	1.077	1.146	1.135
R_1, wR_2 [$I > 2\sigma(I)$]	0.0801, 0.2357	0.0759, 0.2338	0.1149, 0.3019	0.1474, 0.3309	0.0998, 0.2250
R_1, wR_2 [all data]	0.0878, 0.2444	0.0867, 0.2477	0.1415, 0.3286	0.2083, 0.3653	0.1427, 0.2526
$\Delta\rho_{min}/\Delta\rho_{max}$(e·Å^{-3})	1.03/−0.83	0.36/−0.58	1.23/−1.11	0.55/−0.71	0.97/−0.42
CCDC number	2056099	2056100	2056101	2056102	2056103

Table S2. Crystallographic data and structure refinement parameters for two-fold interpenetrated diamond (***dia***) frameworks (**AlOC-104** to **AlOC-108**).

	AlOC-104	**AlOC-105**	**AlOC-106**	**AlOC-107**	**AlOC-108**
Empirical formula	$C_{72}H_{60}Al_4Co_4N_4O_{28}S_{12}$	$C_{72}H_{60}Al_4Co_4N_4O_{28}S_{12}$	$C_{96}H_{84}Al_4Mn_4N_4O_{28}$	$C_{96}H_{84}Al_4Fe_4N_4O_{28}$	$C_{96}H_{84}Al_4Zn_4N_4O_{28}$
Formula weight	2157.68	2157.68	2069.35	2073.07	2111.15
Temperature / K	105.84(14) K	105.89(10) K	293(2) K	99.99(10) K	108.44(10) K
Crystal system	Cubic	Cubic	Cubic	Cubic	Cubic
Space group	*Fd*-3*c*	*Fd*-3*c*	*Fd*-3*c*	*Fd*-3*c*	*Fd*-3*c*
a [Å]	32.0714(6)	32.3326(9)	32.8415(3)	32.3651(4)	32.2437(2)
b [Å]	32.0714(6)	32.3326(9)	32.8415(3)	32.3651(4)	32.2437(2)
c [Å]	32.0714(6)	32.3326(9)	32.8415(3)	32.3651(4)	32.2437(2)
α [°]	90	90	90	90	90
B [°]	90	90	90	90	90
γ [°]	90	90	90	90	90
V [Å^3]	32987.8(19)	33800(3)	35421.7(10)	33902.4(13)	33522.4(6)
Z	15.99936	16	16	15.99936	15.99936
ρ_{calcd} [g cm^{-3}]	1.738	1.696	1.552	1.625	1.673
μ [mm^{-1}]	6.857	6.692	0.684	4.367	1.548
F (000)	17536.0	17536.0	17024.0	17088.0	17344.0
Index ranges	−23 ≤ h ≤ 34 −38 ≤ k ≤ 40 −21 ≤ l ≤ 29	−23 ≤ h ≤ 31 −24 ≤ k ≤ 38 −40 ≤ l ≤ 38	−39 ≤ h ≤ 41 −41 ≤ k ≤ 41 −40 ≤ l ≤ 41	−36 ≤ h ≤ 37 −34 ≤ k ≤ 20 −23 ≤ l ≤ 28	−5 ≤ h ≤ 41 −19 ≤ k ≤ 31 −40 ≤ l ≤ 18
Reflns collected	9190	9024	56347	7286	9994
unique reflns [R_{int}]	1385 [0.0984]	1444 [0.0850]	1522 [0.0798]	1168 [0.0262]	1573 [0.0206]
data/restraints/parameters	1385/6/85	1444/12/94	1522/150/134	1168/219/136	1573/72/134
GOF on F^2	1.308	1.097	1.185	1.051	1.154
R_1, wR_2 [$I > 2\sigma(I)$]	0.1447, 0.3634	0.1274, 0.3121	0.0858, 0.2422	0.0566, 0.1641	0.0548, 0.1676
R_1, wR_2 [all data]	0.2094, 0.4048	0.1813, 0.3512	0.0997, 0.2547	0.0715, 0.1779	0.0568, 0.1697
$\Delta\rho_{min}/\Delta\rho_{max}$(e·Å^{-3})	0.93/−0.75	0.98/−0.94	0.39/−0.46	0.40/−0.48	0.36/−0.43
CCDC number	2056104	2056105	2056106	2156657	2056107

Table S3. Crystallographic data and structure refinement parameters for non-interpenetrated diamond (***dia***) frameworks (**AlOC-109** to **AlOC-111**).

	AlOC-109	**AlOC-110**	**AlOC-111**
Empirical formula	$C_{108}H_{108}Al_4Co_4N_4O_{28}$	$C_{96}H_{84}Al_4Fe_4N_4O_{28}$	$C_{96}H_{84}Al_4Cd_4N_4O_{28}$
Formula weight	2253.62	2072.99	2299.19
Temperature / K	293(2) K	108.56(10) K	108.29(11) K
Crystal system	Cubic	Cubic	Cubic
Space group	$F4_132$	$F4_132$	$F4_132$
a [Å]	32.1474(2)	32.1100(6)	32.8932(3)
b [Å]	32.1474(2)	32.1100(6)	32.8932(3)
c [Å]	32.1474(2)	32.1100(6)	32.8932(3)
α [°]	90	90	90
B [°]	90	90	90
γ [°]	90	90	90
V [Å^3]	33222.9(6)	33107.1(19)	35589.2(10)
Z	8	8	8
ρ_{calcd} [g cm^{-3}]	0.901	0.832	0.858
μ [mm^{-1}]	2.520	2.236	2.882
F (000)	9344.0	8544.0	9248.0
Index ranges	−36 ≤ h ≤ 38 −36 ≤ k ≤ 30 −37 ≤ l ≤ 37	−17 ≤ h ≤ 38 −24 ≤ k ≤ 28 −40 ≤ l ≤ 38	−41 ≤ h ≤ 33 −38 ≤ k ≤ 42 −38 ≤ l ≤ 33
Reflections collected	30287	10983	40255
Independent reflections [R_{int}]	2554 [0.0400]	3067 [0.0465]	3395 [0.1600]
data/restraints/parameters	2554/37/112	3067/2/97	3395/18/103
GOF on F^2	1.062	0.994	1.021
R_1, wR_2 [$I > 2\sigma(I)$]	0.0736, 0.2196	0.0634, 0.1836	0.0751, 0.1956
R_1, wR_2 [all data]	0.0882, 0.2409	0.1068, 0.2120	0.0810, 0.2001
$\Delta\rho_{min}/\Delta\rho_{max}$ (e·Å^{-3})	0.67/–0.31	0.45/–0.26	0.71/–0.62
Flack parameter	0.085(18)	0.082(18)	0.463(13)
CCDC number	2056108	2056109	2056110

Table S4. Crystallographic data and structure refinement parameters for lonsdaleite (***lon***) frameworks (**AlOC-112** to **AlOC-120**).

	AlOC-112	**AlOC-113**	**AlOC-114**	**AlOC-115**	**AlOC-116**	**AlOC-117**	**AlOC-118**	**AlOC-119**	**AlOC-120**
Empirical formula	$C_{96}H_{84}Al_4Co_4N_4O_{28}$	$C_{96}H_{72}Al_4Co_4F_{12}N_4O_{28}$	$C_{96}H_{72}Al_4Co_4Cl_{12}N_4O_{28}$	$C_{108}H_{108}Al_4Co_4N_4O_{28}$	$C_{96}H_{96}Al_4Co_4N_{16}O_{28}$	$C_{96}H_{84}Al_4Mn_4N_4O_{28}$	$C_{96}H_{84}Al_4Fe_4N_4O_{28}$	$C_{96}H_{84}Al_4Zn_4N_4O_{28}$	$C_{96}H_{84}Al_4Cd_4N_4O_{28}$
Formula weight	2085.33	2301.23	2498.64	2253.64	2265.52	2069.35	2073.01	2111.07	2299.21
Temperature / K	298.83 K	105.8(3) K	106.22(10) K	105.78(10) K	109.8(3) K	100.00(18) K	100.00(14) K	293(2) K	108.30(10) K
Crystal system	Hexagonal	Hexagonal	Hexagonal	Hexagonal	Hexagonal	Hexagonal	Hexagonal	Hexagonal	Hexagonal
Space group	*P*-62*c*	*P*-62*c*	*P*-62*c*	*P*-62*c*	*P*-62*c*	*P*-62*c*	*P*-62*c*	*P*-62*c*	*P*-62*c*
a [Å]	22.8201(6)	22.6534(4)	22.7823(2)	22.6942(3)	22.6772(3)	22.9056(5)	22.7862(8)	22.8185(4)	23.1974(5)
b [Å]	22.8201(6)	22.6534(4)	22.7823(2)	22.6942(3)	22.6772(3)	22.9056(5)	22.7862(8)	22.8185(4)	23.1974(5)
c [Å]	37.3225(10)	37.1554(7)	37.2615(5)	37.1096(5)	36.9621(5)	37.4928(8)	37.2553(14)	37.3420(8)	37.9940(7)
α [°]	90	90	90	90	90	90	90	90	90
B [°]	90	90	90	90	90	90	90	90	90
γ [°]	120	120	120	120	120	120	120	120	120
V [Å^3]	16832.0(10)	16512.7(7)	16748.9	16551.8(5)	16461.4(5)	17035.8(8)	16751.8(13)	16838.5(7)	17706.2(8)
Z	3.99996	3.99996	3.99996	3.99996	4	4	3.99996	4	3.99996
ρ_{calcd} [g cm^{-3}]	0.823	0.926	0.991	0.904	0.914	0.807	0.822	0.833	0.863
μ [mm^{-1}]	2.470	2.610	3.651	2.529	2.558	2.939	3.314	0.63	2.897
F (000)	4288.0	4672.0	5056.0	4672.0	4672.0	4256.0	4272.0	4336.0	4624.0
	−20 ≤ h ≤ 23	−20≤ h ≤ 23	−28 ≤ h ≤ 28	−28 ≤ h ≤ 28	−27 ≤ h ≤ 25	−23 ≤ h ≤ 22	−22 ≤ h ≤ 15	−28 ≤ h ≤ 22	−16 ≤ h ≤ 29
Index ranges	−25 ≤ k ≤ 25	−26 ≤ k ≤ 27	−26 ≤ k ≤ 18	−28 ≤ k ≤ 28	−28 ≤ k ≤ 28	−22 ≤ k ≤ 22	−22 ≤ k ≤ 22	−28 ≤ k ≤ 28	−27 ≤ k ≤ 25
	−41 ≤ l ≤ 39	−44 ≤ l ≤ 43	−45 ≤ l ≤ 46	−46 ≤ l ≤ 46	−43 ≤ l ≤ 46	−35 ≤ l ≤ 37	−37 ≤ l ≤ 33	−46 ≤ l ≤ 29	−49 ≤ l ≤ 46
Reflns collected	45568	60558	73594	69421	57708	44069	37180	133920	75940
unique reflns [R_{int}]	8392[0.0657]	10169 [0.0766]	11641 [0.0902]	11455[0.0952]	11074[0.0742]	6229 [0.0538]	6133[0.1182]	11604[0.1270]	12869[0.1057]
data/restraints/parameters	8392/79/403	10169/122/447	11641/67/498	11455/48/511	11074/144/391	6229/0/409	6133/55/409	11604/62/409	12869/2030/361
GOF on F^2	1.073	1.013	1.042	1.064	1.039	1.038	1.068	1.015	1.069
R_1, wR_2 [$I > 2\sigma(I)$]	0.0629, 0.1721	0.0809, 0.2002	0.0757, 0.1927	0.0736, 0.1900	0.0972, 0.2372	0.0576, 0.1595	0.1081, 0.2742	0.0542, 0.1246	0.0784, 0.2148
R_1, wR_2 [all data]	0.0927, 0.1912	0.1194, 0.2235	0.1088, 0.2153	0.0964, 0.2032	0.1467, 0.2771	0.0796, 0.1777	0.1938, 0.3396	0.0765, 0.1395	0.1087, 0.2431
$\Delta\rho_{min}/\Delta\rho_{max}$ (e·Å^{-3})	0.38/–0.28	0.76/–0.38	0.71/–0.37	0.84/–0.38	0.88/–0.29	0.25/–0.30	0.43/–0.57	0.32/–0.28	1.96/–1.70
Flack parameter	0.048(11)	0.150(11)	0.034(7)	0.056(6)	0.104(14)	0.007(7)	-0.006(13)	0.118(12)	0.409(6)
CCDC number	2056111	2056112	2056113	2056114	2056115	2056116	2056117	2056118	2056127

Table S5. BVS analysis for **AlOC-99** to **AlOC-120.**

AlOC-99		**AlOC-100**	
Al1 3.134	Co1 1.854	Al1 3.113	Co1 1.826
Al1—O1 1.896(2)	Co1—O1 1.956(4)	Al1—O1 1.895(3)	Co1—O1 1.958(5)
Al1—O1 1.896(2)	Co1—O3 2.054(3)	Al1—O1 1.895(3)	Co1—O3 2.064(3)
Al1—O1 1.896(2)	Co1—O3 2.054(3)	Al1—O1 1.895(3)	Co1—O3 2.064(3)
Al1—O2 1.886(3)	Co1—O3 2.054(3)	Al1—O2 1.892(3)	Co1—O3 2.064(3)
Al1—O2 1.886(3)	Co1—N1 2.184(6)	Al1—O2 1.892(3)	Co1—N1 2.176(6)
Al1—O2 1.886(3)		Al1—O2 1.892(3)	
AlOC-101		**AlOC-102**	
Al1 3.0159	Co1 1.990	Al1 3.081	Co1 1.927
Al1—O1 1.945(4)	Co1—O1 1.868(7)	Al1—O1 1.898(6)	Co1—O1 1.893(10)
Al1—O1 1.945(4)	Co1—O3 2.056(5)	Al1—O1 1.898(6)	Co1—O2 2.047(8)
Al1—O1 1.945(4)	Co1—O3 2.055(5)	Al1—O1 1.898(6)	Co1—O2 2.047(8)
Al1—O2 1.869(5)	Co1—O3 2.055(5)	Al1—O3 1.896(7)	Co1—O2 2.047(8)
Al1—O2 1.869(5)	Co1—N1 2.170(11)	Al1—O3 1.896(7)	Co1—N1 2.250(14)
Al1—O2 1.869(5)		Al1—O3 1.896(7)	
AlOC-103		**AlOC-104**	
Al1 3.081	Co1 1.856	Al1 3.157	Co1 1.918
Al1—O1 1.891(5)	Co1—O2 1.942(8)	Al1—O1 1.882(6)	Co1—O1 1.970(10)
Al1—O1 1.891(5)	Co1—O3 2.081(5)	Al1—O1 1.882(6)	Co1—O3 2.032(7)
Al1—O1 1.891(5)	Co1—O3 2.081(5)	Al1—O1 1.882(6)	Co1—O3 2.032(7)
Al1—O2 1.892(5)	Co1—O3 2.081(5)	Al1—O2 1.894(7)	Co1—O3 2.032(7)
Al1—O2 1.892(5)	Co1—N1 2.096(10)	Al1—O2 1.894(7)	Co1—N7 2.163(13)
Al1—O2 1.892(5)		Al1—O2 1.894(7)	
AlOC-105		**AlOC-106**	
Al1 3.081	Co1 1.880	Al1 3.157	Mn1 1.934
Al1—O1 1.894(6)	Co1—O2 1.963(10)	Al1—O1 1.889(2)	Mn1—O1 2.029(4)
Al1—O1 1.894(6)	Co1—O3 2.041(7)	Al1—O1 1.889(2)	Mn1—O3 2.132(4)
Al1—O1 1.894(6)	Co1—O3 2.041(7)	Al1—O1 1.889(2)	Mn1—O3 2.132(4)
Al1—O2 1.890(6)	Co1—O3 2.041(7)	Al1—O2 1.899(3)	Mn1—O3 2.132(4)
Al1—O2 1.890(6)	Co1—N1 2.192(14)	Al1—O2 1.899(3)	Mn1—N1 2.256(7)
Al1—O2 1.890(6)		Al1—O2 1.899(3)	
AlOC-107		**AlOC-108**	
Al1 3.147	Fe1 2.006	Al1 3.129	Zn1 1.939
Al1—O1 1.890(2)	Fe1—O1 1.990(4)	Al1—O1 1.8977(16)	Zn1—O2 1.960(3)
Al1—O1 1.890(2)	Fe1—O3 2.077(3)	Al1—O1 1.8977(16)	Zn1—O3 2.059(2)
Al1—O1 1.890(2)	Fe1—O3 2.077(3)	Al1—O1 1.8977(16)	Zn1—O3 2.059(2)
Al1—O2 1.889(3)	Fe1—O3 2.077(3)	Al1—O2 1.8861(19)	Zn1—O3 2.059(2)
Al1—O2 1.889(3)	Fe1—N1 2.190(5)	Al1—O2 1.8861(19)	Zn1—N1 2.178(4)
Al1—O2 1.889(3)		Al1—O2 1.8861(19)	
AlOC-109		**AlOC-110**	
Al1 3.130	Co1 1.845	Al1 3.168	Fe1 2.009
Al1—O1 1.896(3)	Co1—O1 1.959(5)	Al1—O1 1.885(3)	Fe1—O1 1.977(5)
Al1—O1 1.896(3)	Co1—O3 2.058(5)	Al1—O1 1.885(3)	Fe1—O3 2.088(4)
Al1—O1 1.896(3)	Co1—O3 2.058(5)	Al1—O1 1.885(3)	Fe1—O3 2.088(4)
Al1—O2 1.887(4)	Co1—O3 2.058(5)	Al1—O2 1.889(4)	Fe1—O3 2.088(4)
Al1—O2 1.887(4)	Co1—N1 2.172(7)	Al1—O2 1.889(4)	Fe1—N1 2.167(7)
Al1—O2 1.887(4)		Al1—O2 1.889(4)	

AlOC-111			
Al1 3.070	Cd1 2.142		
Al1—O1 1.896(4)	Cd1—O1 2.075(7)		
Al1—O1 1.896(4)	Cd1—O3 2.294(5)		
Al1—O1 1.896(4)	Cd1—O3 2.294(5)		
Al1—O2 1.901(4)	Cd1—O3 2.294(5)		
Al1—O2 1.901(4)	Cd1—N1 2.239(9)		
Al1—O2 1.901(4)			
AlOC-112			
Al1 3.168	Al2 3.168	Co1 1.880	Co2 1.831
Al1—O1 1.902(4)	Al2—O1 1.910(5)	Co1—O5 1.963(10)	Co2—O1 1.946(4)
Al1—O1 1.902(4)	Al2—O1 1.910(5)	Co1—O6 2.041(7)	Co2—O7 2.076(6)
Al1—O1 1.902(4)	Al2—O3 1.888(6)	Co1—O6 2.041(7)	Co2—O9 2.052(5)
Al1—O2 1.897(4)	Al2—O4 1.884(5)	Co1—O6 2.041(7)	Co2—O10 2.058(6)
Al1—O2 1.898(4)	Al2—O5 1.900(4)	Co1—N2 2.192(14)	Co2—N1 2.204(5)
Al1—O2 1.897(5)	Al2—O8 1.890(5)		
AlOC-113			
Al1 3.200	Al2 3.035	Co1 1.844	Co2 1.897
Al1—O1 1.886(5)	Al2—O1 1.885(6)	Co1—O2 2.070(5)	Co2—O1 1.941(5)
Al1—O1 1.886(5)	Al2—O1 1.910(5)	Co1—O2 2.070(5)	Co2—O7 2.040(6)
Al1—O1 1.886(5)	Al2—O3 1.891(4)	Co1—O2 2.070(5)	Co2—O8 2.049(7)
Al1—O9 1.880(6)	Al2—O4 1.906(6)	Co1—O3 1.962(6)	Co2—O10 2.063(7)
Al1—O9 1.880(6)	Al2—O5 1.917(5)	Co1—N1 2.117(7)	Co2—N2 2.164(7)
Al1—O9 1.880(6)	Al2—O6 1.908(5)		
AlOC-114			
Al1 3.109	Al2 3.141	Co1 1.920	Co2 1.855
Al1—O1 1.888(5)	Al2—O2 1.894(4)	Co1—O3 1.984(7)	Co2—O2 1.965(4)
Al1—O2 1.886(5)	Al2—O2 1.894(4)	Co1—O9 2.039(6)	Co2—O6 2.034(6)
Al1—O2 1.914(5)	Al2—O2 1.894(4)	Co1—O9 2.039(6)	Co2—O7 2.063(6)
Al1—O3 1.888(4)	Al2—O5 1.886(5)	Co1—O9 2.039(6)	Co2—O10 2.050(6)
Al1—O4 1.895(6)	Al2—O5 1.886(5)	Co1—N2 2.105(8)	Co2—N1 2.188(6)
Al1—O8 1.892(6)	Al2—O5 1.886(5)		
AlOC-115			
Al1 3.104	Al2 3.077	Co1 1.917	Co2 1.903
Al1—O1 1.894(4)	Al2—O1 1.903(5)	Co1—O1 1.950(4)	Co2—O2 1.962(6)
Al1—O2 1.894(4)	Al2—O1 1.899(5)	Co1—O7 2.033(5)	Co2—O3 2.042(5)
Al1—O2 1.894(4)	Al2—O2 1.895(3)	Co1—O9 2.053(5)	Co2—O7 2.042(5)
Al1—O3 1.895(4)	Al2—O5 1.897(5)	Co1—O10 2.033(5)	Co2—O10 2.042(5)
Al1—O4 1.895(4)	Al2—O6 1.896(4)	Co1—N1 2.168(5)	Co2—N1 2.153(8)
Al1—O8 1.895(4)	Al2—O8 1.896(5)		
AlOC-116			
Al1 3.078	Al2 3.160	Co1 1.932	Co2 1.909
Al1—O1 1.904(5)	Al2—O1 1.895(6)	Co1—O3 1.918(9)	Co2—O1 1.947(5)
Al1—O1 1.904(5)	Al2—O1 1.886(6)	Co1—O6 2.041(7)	Co2—O8 2.062(7)
Al1—O1 1.904(5)	Al2—O2 1.874(6)	Co1—O6 2.041(7)	Co2—O9 1.992(9)
Al1—O4 1.891(5)	Al2—O3 1.905(5)	Co1—O6 2.041(7)	Co2—O10 2.075(8)
Al1—O4 1.891(5)	Al2—O5 1.894(6)	Co1—N2 2.206(11)	Co2—N1 2.177(7)
Al1—O4 1.891(5)	Al2—O7 1.873(7)		
AlOC-117			

Al1 3.153	Al2 3.114	Mn1 2.028	Mn2 2.015
Al1—O1 1.887(5)	Al2—O1 1.888(6)	Mn1—O4 2.004(8)	Mn2—O1 1.997(5)
Al1—O1 1.887(5)	Al2—O1 1.902(6)	Mn1—O9 2.130(6)	Mn2—O7 2.133(7)
Al1—O1 1.887(5)	Al2—O3 1.915(6)	Mn1—O9 2.130(6)	Mn2—O8 2.132(7)
Al1—O2 1.890(6)	Al2—O4 1.893(4)	Mn1—O9 2.130(6)	Mn2—O10 2.152(8)
Al1—O2 1.890(6)	Al2—O5 1.880(5)	Mn1—N1 2.200(11)	Mn2—N2 2.196(6)
Al1—O2 1.890(6)	Al2—O6 1.882(6)		
AlOC-118			
Al1 3.088	Al2 3.064	Fe1 1.919	Fe2 2.231
Al1—O1 1.936(12)	Al2—O1 1.876(13)	Fe1—O4 2.02(2)	Fe2—O1 1.958(10)
Al1—O1 1.936(12)	Al2—O1 1.896(14)	Fe1—O9 2.094(13)	Fe2—O7 2.057(16)
Al1—O1 1.936(12)	Al2—O2 1.922(16)	Fe1—O9 2.094(13)	Fe2—O8 2.036(15)
Al1—O3 1.861(13)	Al2—O4 1.878(11)	Fe1—O9 2.094(13)	Fe2—O10 2.03(2)
Al1—O3 1.861(13)	Al2—O5 1.924(14)	Fe1—N1 2.18(3)	Fe2—N2 2.128(14)
Al1—O3 1.861(13)	Al2—O6 1.904(11)		
AlOC-119			
Al1 3.014	Al2 3.066	Zn1 1.828	Zn2 1.880
Al1—O1 1.897(3)	Al2—O1 1.900(4)	Zn1—O6 1.991(5)	Zn2—O1 1.967(3)
Al1—O1 1.897(3)	Al2—O1 1.899(4)	Zn1—O4 2.079(4)	Zn2—O7 2.081(4)
Al1—O1 1.897(3)	Al2—O2 1.912(4)	Zn1—O4 2.079(4)	Zn2—O9 2.075(4)
Al1—O3 1.914(3)	Al2—O4 1.903(3)	Zn1—O4 2.079(4)	Zn2—O10 2.079(4)
Al1—O3 1.914(3)	Al2—O5 1.889(3)	Zn1—N2 2.189(6)	Zn2—N1 2.166(4)
Al1—O3 1.914(3)	Al2—O6 1.892(4)		
AlOC-120			
Al1 3.119	Al2 2.978	Cd1 2.206	Cd2 2.211
Al1—O2 1.887(6)	Al2—O1 1.901(8)	Cd1—O5 2.057(9)	Cd2—O2 2.084(5)
Al1—O2 1.887(6)	Al2—O2 1.894(8)	Cd1—O7 2.279(8)	Cd2—O8 2.284(8)
Al1—O2 1.887(6)	Al2—O2 1.890(8)	Cd1—O7 2.279(8)	Cd2—O9 2.271(8)
Al1—O3 1.898(6)	Al2—O4 1.907(7)	Cd1—O7 2.279(8)	Cd2—O10 2.258(8)
Al1—O3 1.898(6)	Al2—O5 1.904(5)	Cd1—N2 2.247(12)	Cd2—N1 2.226(7)
Al1—O3 1.898(6)	Al2—O6 1.966(7)		

Table S6. Direct aldol reactions catalyzed by **AlOCs**.[a]

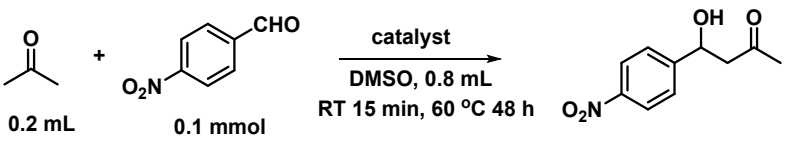

0.2 mL 0.1 mmol

Entry	catalyst	yield/ %
1	**AlOC-99 (10 mol%)**	79% [b]
2	**AlOC-109 (10 mol%)**	87% [b] (88% [c])
3	**AlOC-112 (10 mol%)**	88% [b]
4	**AlOC-99 (5 mol%)**	48% [b]
5	**AlOC-109 (5 mol%)**	67% [b]
6	**AlOC-112 (5 mol%)**	68% [b]
7	**Without Catalyst**	none

[a] Firstly, the mixed solution of catalyst, acetone (0.2 mL) and DMSO (0.8 mL) was stirred at room temperature for 15 min. Then, 4-nitrobenzaldehyde (0.1 mmol) was added and the solution further stirred at 60 °C for 48h. [b] The yield of the isolated product based on 4-nitrobenzaldehyde. [c] The yield of isolated product based on 4-nitrobenzaldehyde after three runs.

References

[1] T. Ge, C. Zuo, H. Chen, Y. Muhammad, L. Wei, C. Li, *Ind. Eng. Chem. Res.* **2019**, *58*, 3595-3605.
[2] H.-L. Zheng, S.-L. Huang, M.-B. Luo, Q. Wei, E.-X. Chen, L. He, Q. Lin, *Angew. Chem. Int. Ed.* **2020**, *59*, 23588-23592.
[3] W. Zheng, R. Tan, L. Zhao, Y. Chen, C. Xiong, D. Yin, *RSC Adv.* **2014**, *4*, 11732-11739.
[4] Q. Wang, M. Liao, Z. Mu, X. Zhang, H. Dong, Z. Liang, J. Luo, Y. Yang, F. Wu, *J. Phys. Chem. C* **2020**, *124*, 886-895.
[5] N. Andreu, D. Flahaut, R. Dedryvère, M. Minvielle, H. Martinez, D. Gonbeau, *ACS Appl. Mater. Interfaces* **2015**, *7*, 6629-6636.
[6] H. Virieux, M. Le Troedec, A. Cros-Gagneux, W.-S. Ojo, F. Delpech, C. Nayral, H. Martinez, B. Chaudret, *J. Am. Chem. Soc.* **2012**, *134*, 19701-19708.
[7] Z. Zhang, M. Zhang, X. Li, K. Li, X. Lü, Y. Wang, X. Zhu, *ACS Sustainable Chem. Eng.* **2018**, *6*, 11614-11623.
[8] Z. J. Yu, M. Rajesh Kumar, Y. Chu, H. X. Hao, Q. Y. Wu, H. D. Xie, *ACS Sustainable Chem. Eng.* **2018**, *6,* 155-164.
[9] Y. Quan, W. Shi, Y. Song, X. Jiang, C. Wang, W. Lin, *J. Am. Chem. Soc.* **2021**, *143*, 3075-3080.
[10] G. K. Mor, T. P. Le, K. Vakhshouri, D. R. Kozub, E. D. Gomez, *ACS Appl. Mater. Interfaces* **2014**, *6*, 19638−19643.